DESIGN AND MODELING OF HIGH PERFORMANCE LED DIMMING DRIVER WITH REDUCED CURRENT SPIKES USING TURN-ON SNUBBER ACROSS POWER MOSFET

by

Venkata Shesha Vamsi Borra

Submitted in partial Fulfillment of the Requirements

for the Degree of

Master of Science

in the

Electrical Engineering

Program

YOUNGSTOWN STATE UNIVERSITY

May, 2014

Design and Modeling of High Performance LED Dimming Driver with Reduced Current Spikes using Turn-On Snubber across Power MOSFET

Venkata Shesha Vamsi Borra

I hereby release this thesis to the public. I understand that this thesis will be made available from the OhioLINK ETD Center and the Maag library Circulation Desk for public access. I also authorize the University or other individuals to make copies of this thesis as needed for scholarly research.

Signature:

_____

Venkata Shesha Vamsi Borra, Student Date

Approvals:

_____

Dr. Frank X. Li, Thesis Advisor Date

_____

Dr. Faramarz Mossayebi, Committee Member Date

_____

Dr. Jalal Jalali, Committee Member Date

_____

Dr. Salvatore A. Sanders, Associate Dean Graduate Studies Date

Abstract

The LEVEL-3 power MOSFET SPICE model (IRF034) is used to design and model the LED driver. Three LED drivers are designed and their efficiency values are compared for picking the optimum driver among them. The switching frequency of 20 kHz to 40 kHz to the MOSFET indeed produce sharp current spikes across the MOSFET which are at least 30-40 times more than the desired value around 2A. To resolve this problem an efficient turn-on Snubber circuit is designed for the driver for safe operation.

The efficiency of the LED driver is enhanced by modeling the LED's PSpice model and reconfiguring the circuit elements. The simulation results of the designed driver propose an efficiency value of 92.2%. The efficiency is calculated to be 88% when the designed model is replaced by a commercial LED model.

Acknowledgements

First and foremost, I would like to thank God for giving me wisdom and guidance for doing this research.

I would like to express my sincere gratitude and thanks to Dr. Frank X. Li for his invaluable support and guidance. I have been extremely lucky to have exceptional mentors who helped me to gain self-confidence and enthusiasm to complete this thesis: Dr. Faramarz Mossayebi, who was always a great moral support and helped me to stay cheerful; Jim Cook, whose was both a mentor and a friend: I owe you much more than you realize.

I would like to thank the staff of the Electrical and Computer Engineering Department for all the support I received: Dr. Jalal Jalali, Dr. Salvatore Pansino, Roslyn Pozega and especially Dr. Phil Munro for taking time for reviewing my thesis manuscript.

Finally, words fail me in expressing my gratitude to my family. I might not have made it to the end without the support from my parents Mr. Rama Mohan Borra and Mrs. Kumari Borra, my brother Mr. Chaitanya Borra, family and friends.

Table of Contents

List of Figures

List of Tables

Abbreviations

AC	Alternating Current
BJT	Bipolar Junction Transistor
CSV	Comma-Separated Values
DC	Direct Current
EMI	Electromagnetic Interference
IGBT	Insulated-Gate Bipolar Transistor
IRF	International Rectifier
LED	Light Emitting Diode
MOSFET	Metal-Oxide-Semiconductor Field-Effect Transistor
PER	Period
PSU	Power Supply Unit
PW	Pulse Width
PWM	Pulse Width Modulation
RC	Resistor-Capacitor
RCD	Resistor-Capacitor-Diode
RGB	Red, Green and Blue
SPICE	Simulation Program with Integrated Circuit Emphasis

Chapter 1

Introduction

Light Emitting diodes (LEDs) lighting technology was developed as a result of humanity's quest for finding more and more efficient and environmentally-friendly solutions. Analogous to the flex-fuel and hybrid technologies for automobiles, which are solutions to alleviate environmental damage (i.e., mitigate strain on world resources), LEDs are the replacement for the present fluorescent and other types of traditional lighting technologies.

LEDs have become a popular light source due to their advantages such as high luminous efficacy, long lifetime, high compactness, efficient conversion of energy, and good color rendering [1] [2] [3] [4] [5] [6] [7] . According to Dave Cooper [8], the demand for LED dimming applications is increasing due to the expanded use of LEDs in general. LEDs generally need drivers to supply the rated and required amount of current. Any current which is more than the rated current will negatively affect the life of the LED. Three driver circuits were developed during the course of this research. The challenge in designing an LED driver is to make it more efficient and flexible with any diode arrangement. Therefore efficiency and device protection are the top priority topics of discussion in this entire thesis. The essential circuits have been designed and tested on SPICE simulation software to compare the efficiency. Controlling the spikes and shrinking the time-delay were also concerns faced in this work.

1.1 Background

Since the scope of dimming applications has seen a dramatic surge over the past few years, the demand in developing more efficient LED dimming drivers has been growing in a same pace. Dimming is not only used in mood lighting, but also used as a means to further decrease the energy consumption by only supplying light at an intensity that is necessary. For instance, lights in a parking garage or residential street may be dimmed to a low level late at night and only brought up to full brightness if a motion sensor detects any movement. Lights over a wide area may be connected together using wireless technology to form a local network, using complex sensing, control and monitoring capability through software to enhance the light levels for all circumstances. The fact that LEDs react rapidly to changes in input power allows one to apply this type of control in a broader sense, with the possibility for dramatic improvements in energy consumption. In contrast, earlier lighting methods such as metal halide or cold cathode gas-discharge technologies react very slowly and are not practical to control brightness in real time. The ability for dimming can therefore be considered to be a crucial element in the general acceptance and use of LED lighting, Portable devices which use LED-based lighting and dimming options for adjusting the light output for the ambient lighting environments require an efficient driver that extends battery life. Dimming is very essential in applications such as portable GPS navigation systems or the backlight for smart phones to guarantee an easily readable display in all ambient lighting conditions. In flashlights, a user might consider longer battery life more vital than delivering the most light possible [9]. Some other LED dimming applications are discussed in the second chapter.

The power MOSFET is used as a switch in this PWM method to control the average amount of power through the LED. Since this MOSFET is operated at frequency range of 20 kHz to 40 kHz, huge current spikes are caused due to the parasitic capacitance and inductance across the MOSFET. Much research has been conducted and many papers have been published to determine the methods to decrease these current spikes across the MOSFET, which would then reduce stress and prevent premature failure. One such experiment is detailed in this study.

1.2 Basics of the Research

Dimming in LEDs is accomplished by two methods: analog dimming and pulse-width modulation (PWM). This thesis inclines towards designing and modeling an LED dimming driver using the PWM method as this method has many advantages, which are discussed in second chapter. Figure 1 (a) shows the basic schematic of how a pulse width modulated LED driver is operated. The switch (SW3) is controlled by a control pulse which is varied according to the different levels of brightness needed. Figure 1 (b) illustrates the analog dimming circuit.

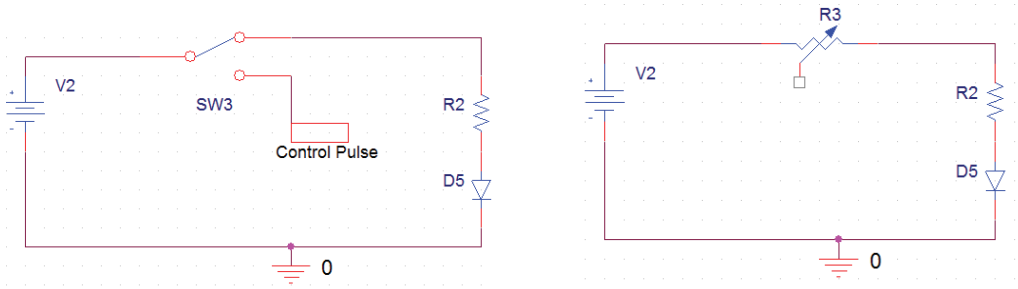

Figure 1: Schematic of (a) PWM LED driver, (b) Analog LED driver

For the PWM method the average current is related approximately to peak current according to the following equation.

$$I_{AVG} = I_{PEAK} * D \quad (1)$$

Where

$D = \frac{t_{on}}{T} = Duty\ Cycle$

$t_{on} = Switch\ on\ time$

$T = switching\ period$

In this thesis, three separate driver configurations are presented. Then the most efficient configuration that is chosen for further research into improving the efficiency. The remainder of the thesis is devoted to presenting the design of a snubber circuit which was created in order to control the current spikes caused by the stray capacitances across the terminals of the MOSFET. The turn-on snubber will be introduced and the design will be shown for the chosen circuit. Near the end of the thesis, efficiency of the driver circuit is discussed in terms of modeling the LEDs SPICE parameters to achieve the highest efficiency. The modeled LEDs SPICE parameters were replaced by the commercially available SPICE parameters in order to compare the efficiency and check the practicality of the driver.

1.3 Organization

This work is divided into four chapters following this one. Chapter 2 provides an overview of two dimming techniques and their advantages including a summary of SPICE models of diodes and MOSFETs. Chapter 3 covers the design of drivers and their efficiency calculation method and the need for designing the snubber circuit. Chapter 4

introduces the different available snubbers, methods for designing them, modeling the SPICE diode model, and a comparison with the available commercial LED model. The conclusion and future work is stated in the last chapter.

Chapter 2

Dimming methodologies and SPICE models

This chapter covers the basic dimming methods and their advantages with the detailed explanation of the SPICE simulation software diode models that are used in later chapters for increasing the overall driver efficiency.

2.1 Dimming Methods

LEDs cannot be used directly, but must be mounted onto a circuit board that provides physical support, interconnection and cooling. The whole assembly of LEDs on the circuit board is normally referred to as a *light engine*, which is cooled by using a *heat-sink*. LEDs must be supplied with a DC current that is accurately controlled to provide the required light level without exceeding the LED rating. The current control function is provided by a driver. A *power supply unit* (PSU) converts the AC into DC for the driver, and provides safety isolation. Figure 2 below shows a rough block diagram.

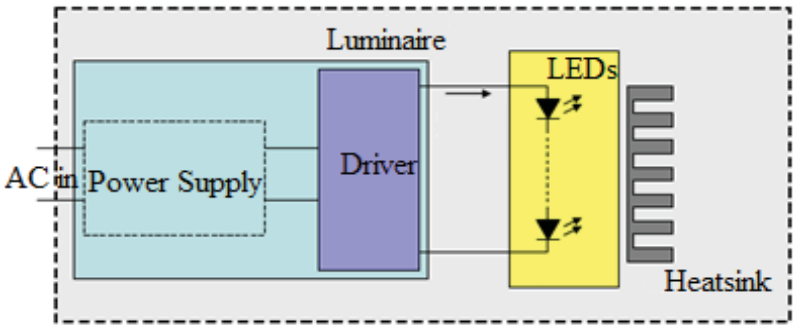

Figure 2 : LEDs with its driver and power supply unit

The fact that LEDs react rapidly to changes in input power allows the application of this kind in broader sense, with the possibility for dramatic improvements in energy

consumption. There are generally two basic methods to control the brightness (i.e., light output) of the LEDs:

1. Analog Dimming
2. Pulse Width Modulation (PWM) Dimming

2.1.1 Analog Dimming

This type of dimming is very straight forward and not sophisticated in operation. In this method the drive current fed to the LEDs is controlled linearly to cause the dimming. Analog dimming is illustrated below.

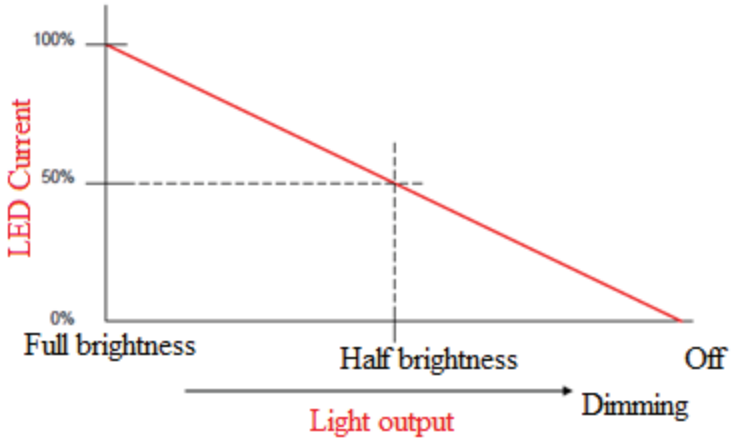

Figure 3: Linear current control in analog dimming

In this method the commonly used form of brightness control for lighting is the triac-based dimmer which is in extensive use in many applications. Although this method is very easy to implement, overall performance is not very great as most of the energy is lost across the variable resistor, which is the key for analog dimming. Also, the color temperature changes as the driver current varies, which is one of the major disadvantages.

2.1.2 Pulse Width Modulation (PWM) Dimming

The foremost benefit of PWM is that power loss in the switching devices is very low. When a switch is in off position there is almost zero current, and when it is in the on position, there is practically no voltage drop across the switch. Power dissipation, being the product of current and voltage, is thus in both cases close to zero. Equations 2 and 3 describe the typical PWM waveform shown in the Figure 4.

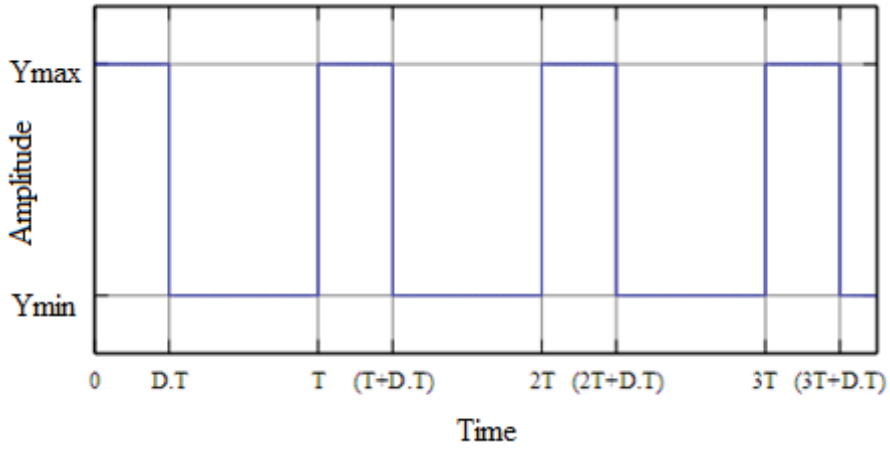

Figure 4: Pulse wave with y_{max} and y_{min} as maximum and minimum values

$$y' = \left(\frac{1}{T}\right) * \left(\int_0^{D*T} y_{max} dt + \int_{D*T}^{T} y_{min} dt \right) \quad (2)$$

$$y' = D * y_{max} + (1 - D) y_{min} \quad (3)$$

where

$D = \frac{t_{on}}{T} = Duty\ Cycle$

$D * T = Switch\ ON\ time$

$T = Switching\ period$

$y' = Average\ value\ of\ the\ waveform$

This type of dimming depends on the capability of the human eye to integrate the average amount of light in the pulses. Duty cycle of the pulse plays a vital role in changing the average current through the LED which indeed influences the brightness. In PWM dimming the amplitude of the pulses always remain the same, only the width is varied accordingly to control the brightness. The graph in Figure 5 is an example of a PWM control signal. Here, in this case the ON-time and OFF-time are equal, so the average current is 50% of the total current. In this case the LEDs are at 50% of the maximum brightness. Similarly, for much lower brightness the LEDs can be driven only 25% of the time as in Figure 6.

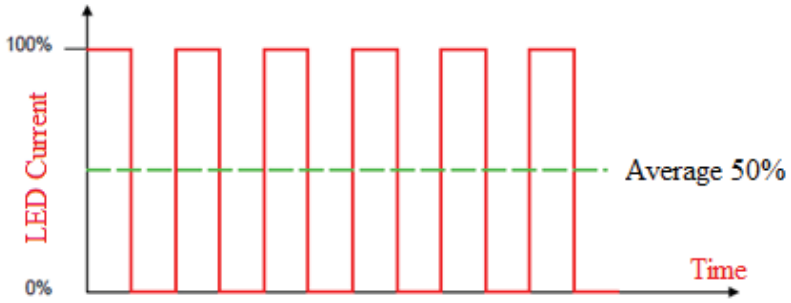

Figure 5: PWM control signal with 50% duty cycle

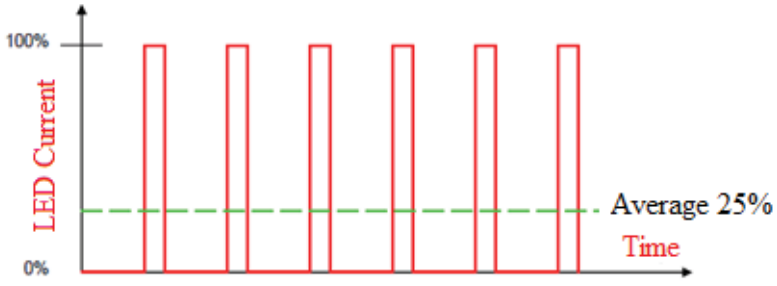

Figure 6: PWM control signal with 25% duty cycle

The main advantage of this PWM dimming is that it maintains very high efficiency without compromising the color temperature. In this type LEDs are always either ON or OFF, since there is no intermediate stage. Similarly, the color temperature is always constant for any brightness level since there is no intermediate state. Normally a pulse rate of approximately 200 Hz is high enough to achieve this objective, without any visible flickering. Also, the PWM drivers provide very precise output levels. For these reasons, PWM is considered in this study for examining the characteristics of the circuits which are built in PSPICE environment.

Although there are many dimming controls like DALI [10], DMX [11] and ZIGBEE [12], the basic principle is either Analog or PWM diming in every case.

2.1.3 Major Applications of Dimming

LEDs and light engines do not need to deliver full brightness every time they are lit up. For example, LED TVs which use LEDs as their backlight require local dimming to improve the visibility of bright and dark images on the TV screen. In Figure 7 it is very clear how the different dimming designs can influence the quality of the images or scenes on a TV. In Figure 7(a), the quality of image is not very clear as the dimming drivers are positioned only at the corners of the screen. However in Figure 7(b) the images are very clear compared to the Figure 7(a) because of its full-array local dimming.

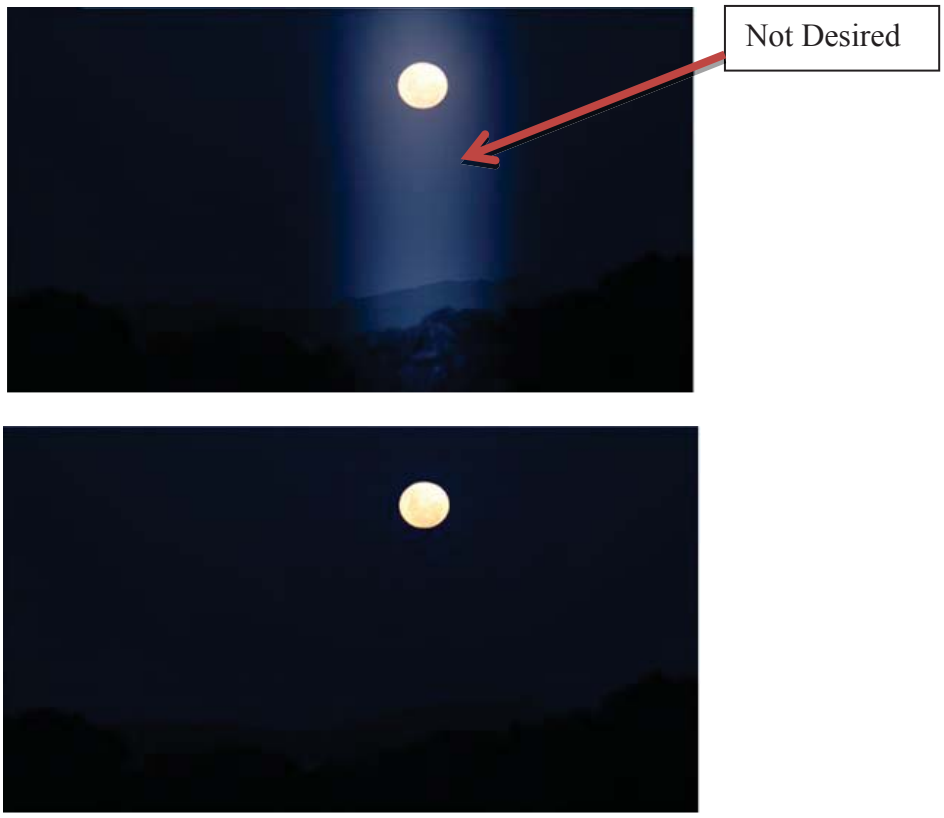

Figure 7 :(a) Dimming control at corners of the screen, (b) Full- array local dimming

This major difference generally occurred because of the positions of the drivers and also number of drivers used for producing this effect. Figure 8 is an example of edge-lit LED TV.

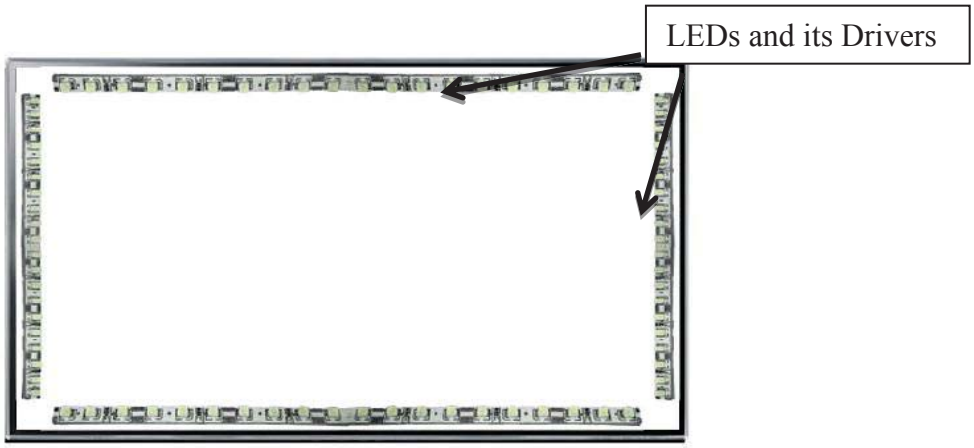

Figure 8: Edge - lit LED TV

Similarly the dimmers are required in applications such as the backlight for electronic and portable gadgets to guarantee a clear display in different light situations.

2.2 SPICE simulation Software

Electronics Research Laboratory of the University of California, Berkeley developed the SPICE software in 1973. It is not practical to build complex circuit models on a breadboard before manufacturing it, so simulating the circuit with SPICE is a brilliant way to verify circuit operation at the basic level before manufacturing any complex circuit.

Every circuit element SPICE model includes parameters which describe the behavior of that element in real world. The number of parameters in a model increases depending upon the level of simulation and degree of accuracy. All the components that are used in the simulation process are predesigned with the parameters that mathematically define the functionality of that component that imitates the real world behavior. SPICE inspired and served as a basis for many other circuit simulation programs, in academia, in industry, and in commercial products [13]. Many manufacturers are now offering SPICE models of their products to designers for verifying the compatibility and accuracy in the designed circuits with their products.

Modeling is another important tool offered in SPICE for a designer or researcher to model the components that suit their needs. Cadence - OrCAD PSpice 16.5 [14] was used in this thesis as a simulation tool for designing the LED driver and modeling the diode SPICE models.

2.2.1 Diode SPICE model

The SPICE model of an Diode model consists of mathematical equations, parameters, and variables, all of which are designed to work together to simulate as accurately as possible the electrical characteristics of a real device [15] [16].

Parameters for an Diode spice model are given in Table 1 [17]. Generally there are four model groups that are responsible for simulating various Diode characteristics. These groups consist of the large-signal dc model, the small-signal ac model, temperature and area effects and the noise model.

Table 1: Diode SPICE Model Parameters

Name	Parameter	Units	Default	Example
IS	saturation current	A	1.0e-14	1.0e-14
RS	ohmic resistance	Ω	0	10
N	emission coefficient	-	1	1.0
TT	transit-time	sec	0	0.1ns
CJO	zero-bias junction capacitance	F	0	2pF
VJ	junction potential	V	1	0.6
M	Junction capacitance grading coefficient	-	0.5	0.5
EG	activation energy	eV	1.11	1.11(Si)
XTI	Saturation-current temp. exp	-	3.0	3.0 (pn) 2.0 (Schottky)
KF	flicker noise coefficient	-	0	
AF	flicker noise exponent	-	1	
FC	coefficient for forward-bais depletion capacitance formula	-	0.5	
BV	reverse breakdown voltage	V	infinite	40.0
IBV	current at breakdown voltage	A	1.0e-3	
TNOM	parameter measurement temperature	deg C	27	50

Simple DC equation for a diode is given by the Shockley equation:

$$Id = Is * \left\{ e^{\left(\frac{Vd}{N*Vt}\right)} - 1 \right\} \quad (4)$$

where

Id = Diode Current

Is = Diode's reverse saturation current

Vd = Applied voltage across the diode

Vt = Thermal voltage

N = Emission coefficient of a diode

The large-signal behavior of the SPICE diode is characterized by the relationship between the dc current and the voltage at its terminals. The parameters used to model this behavior are IS, RS, N, BV and IBV. The parameter IS is the same as the reverse saturation current I_s for an ideal diode. The ohmic resistance RS is used to model the resistance of the metal contacts and the neutral regions under high-level injection. The emission coefficient N is used to modify the slope of the current versus voltage (I-V) characteristics curve. Finally, the parameters BV and IBV model the reverse breakdown behavior.

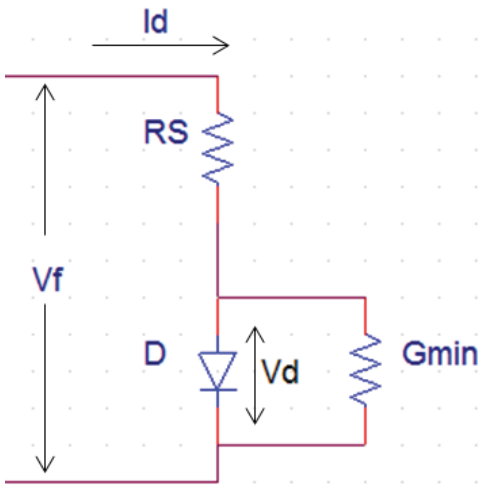

Figure 9: Large-signal DC model

The Figure 9 [15] is an equivalent circuit of the SPICE diode for large-signal dc analysis. Here, it contains internal diode D, a series resistance having a value of RS, and a shunt conductance Gmin. The SPICE program adds this conductance, which is transparent to the user, around every internal pn junction to aid convergence. The default value for Gmin is 10^{-12} mhos.

The dc model consists of the voltage across the external diode terminals Vf, the voltage across the internal diode terminals Vd, and the terminal current Id. From these parameters the characteristics are modeled by the following equations

$$V_f = RS * Id + Vd \tag{5}$$

$$Id = f(Vd) \tag{6}$$

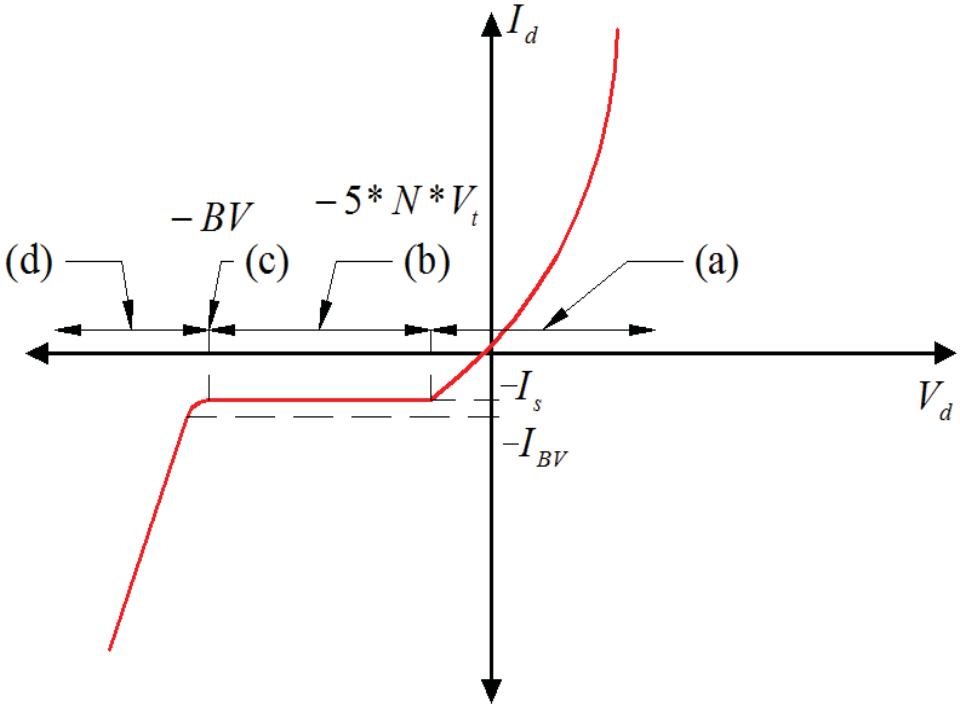

Figure 10: Large-signal I-V Characteristics of the SPICE Diode Model

The four regions of operation in Figure 10 describe the practical relationship between the internal diode voltage and diode current.

For Region (a): $V_d \geq -5 * N * V_t$

$$Id = Is * \left\{ e^{\left(\frac{Vd}{N*Vt}\right)} - 1 \right\} + Gmin * Vd \tag{7}$$

For Region (b): $-BV < V_d < -5 * N * V_t$

$$Id = -Is + Gmin * Vd \tag{8}$$

For Region (c): $V_d = -BV$

$$Id = -IBV \tag{9}$$

For Region (d): $V_d < -BV$

$$Id = Is * \left\{ e^{\left(\frac{-(BV+Vd)}{Vt}\right)} - 1 \right\} + \frac{BV}{Vt} \tag{10}$$

V_t is the thermal voltage which is defined as

$$V_t = \frac{k * T}{q} = 25mV$$

for

$k = 1.38 * 10^{-23} J/K$, T = 300 K, $q = 1.6 * 10^{-19}\ C$

Plots for these four regions are illustrated in Figure 10.

In the Small-Signal AC model, the circuit elements included are junction capacitance CJ, the dynamic conductance GD, and the diffusion capacitance CD, all of which are bias dependent as are those corresponding elements of the ideal diode model.

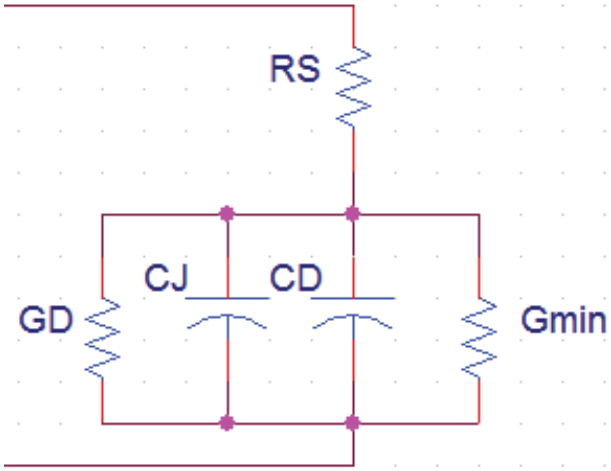

Figure 11: Small-signal SPICE Diode model

Figure 11is an equivalent circuit of the SPICE diode for small-signal AC analysis. The junction capacitance is modeled by the parameters CJO, VJ, M and FC. The parameters CJO and VJ are identical to the zero-bias junction capacitance $C_j(0)$ and the contact potential V_j described for an ideal diode. The parameter M is a grading exponent that is used to change the slope of the junction capacitance versus voltage characteristics curve. The parameter FC is used to model the capacitance under forward bias condition.

The variables for the model are the junction capacitance CJ in farads and the internal diode voltage Vd which is related by

$$CJ = CJO * \{ 1 - \frac{Vd}{VJ} \}^{-M}$$

Temperature behavior of the SPICE diode is modeled through certain temperature dependent parameters like IS, VJ, CJO and FC. Nominal temperature which is represented by TNOM has a default value of 27 ºC. Also, SPICE considerers all input data and the model parameters have been defined at 27 ºC.

The saturation current IS and junction voltage/contact potential VJ are modeled by using the parameters N, EG and XTI for their temperature dependency.

$$IS(T) = IS(TNOM) * (\frac{T}{TNOM})^{\frac{XTI}{N}} * e^{[\frac{q*EG}{N*k}]*[\frac{1}{TNOM}-\frac{1}{T}]} \quad (11)$$

$$VJ(T) = VJ(TNOM) * \left(\frac{T}{TNOM}\right) + \frac{2*k*T}{q} * \ln(\frac{n_i(TNOM)}{n_i(T)}) \quad (12)$$

where

IS (TNOM), VJ (TNOM) = nominal values of saturation current

IS (T), VJ (T) = evaluated values at the analysis temperature T

n_i(T) is the intrinsic carrier concentation in cm^{-3}

Some parameters like IS, RS, CJO and IBV are functions of the junction area(AREA). They are related by the following equations:

$$IS = AREA * IS \quad (13.a)$$

$$RS = \frac{RS}{AREA} \quad (13.b)$$

$$CJO = AREA * CJO \quad (13.c)$$

$$IBV = AREA * IBV \tag{13.d}$$

AREA has a default value of 1.

Noise behavior of a SPICE diode is modeled by adding two noise current sources added to the small-signal ac circuit model, which is illustrated in Figure 12.

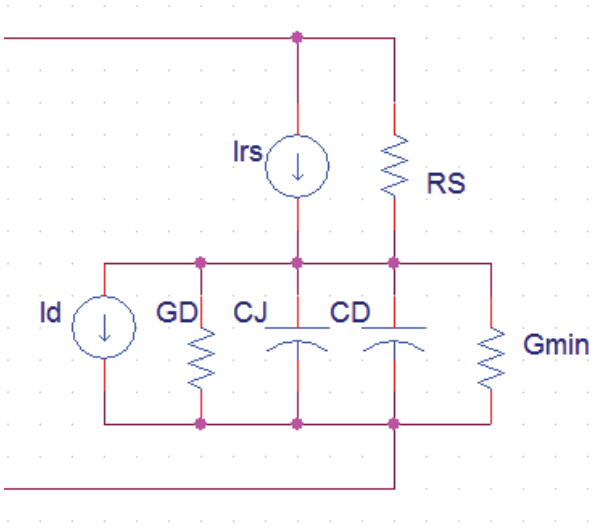

Figure 12: Small-signal SPICE Diode model with Noise Sources

The current source Irs is responsible for modeling thermal noise generated by the resistance RS. The mean-squared value of thermal noise current generated by this source is expressed as

$$\overline{\iota_{RS}{}^2} = \frac{4 * k * T}{RS} * \Delta f \tag{14}$$

Where

T= Temperature in ºK

Δf = Noise bandwidth in Hz

The current Source Id is responsible for modeling both shot and flicker niose generated in the depletion region of the diode.They are related by the following expression

$$\overline{\iota_{RS}{}^2} = 2 * q * Id * \Delta f + KF * \frac{I_d{}^{AF}}{f} * \Delta f \quad (15)$$

Where

Id= diode DC current

f= frequency at which noise is mesured

AF, KF = SPICE flicker noise parameters

PSPICE Diode models are shown below:

```
.model D02bz2_2 D (Is=10.01E-21 N=1.962 Rs=1.603 Ikf=11.45m
Xti=3 Eg=1.11 Cjo=1p
+          M=.3333 Vj=.75 Fc=.5 Isr=7.539u Nr=2 Bv=2.188
           Ibv=11.84m
+          Tt=14.43n)

.model MBR030 D (Is=12.29n Rs=0.102 Ikf=15.89m N=1 Xti=0
Eg=1.11 Cjo=90p
+         M=.1112 Vj=.75 Fc=.5 Isr=1.977u Nr=2)
*         Motorola   pid= MBR030    case=DO35
*         88-09-15 rmn
```

The SPICE model of LED manufactured by the OSRAM semiconductors is included in the LED modeling to estimate the real efficiency of the designed driver. The LED model and its parameters are detailed in the later chapters.

2.2.2 MOSFET SPICE model

Before selecting an appropriate MOSFET model in analysis, one must know the electrical parameters that are critical to that specific application.

MOSFET models are of two types: p-channel or n-channel model; they are categorized according to different levels of sophistication, such as LEVEL - 1 (simple) or LEVEL - 25 (complex). As per HSPICE MOSFET models manual there are 64 different

levels of MOSFET models developed. Synopsys has developed and adapted all these 64 different levels of MOSFET models for use with HSPICE [18].

The complexity and the number of electrical parameters increase as we move to higher level models. Higher levels have more robustness and fewer convergence problems. If higher precision is required, the use of more detailed models, such as the LEVEL - 6 IDS model or one of the BSIM models (LEVEL 13, 28, 39, 47, 49, 53, 54, 57, 59, and 60) is highly recommended.

LEVEL - 1 model is used very often to simulate large digital circuits in situations where detailed analog models are not needed. LEVEL - 1 models offer low simulation time and a relatively high level of accuracy for timing calculations. LEVEL - 2 model was developed as the improvement to the LEVEL - 1. This model describes the effect of channel length modulation, carrier velocity saturation and mobility degradation. In order to overcome the convergence problems in LEVEL - 2, LEVEL - 3 models have been developed. Also it requires even less simulation time and it includes the drain-induced barrier lowering effect-ETA parameter. These are impressively physical, modeling two-dimensional effects based on junction depth and depletion depths.

Table 2 [19] gives all the parameters that are included in the MOSFET LEVEL - 3 SPICE model. Figure 13 [20] is a schematic of a typical MOSFET model.

Table 2: Level 3 MOSFET SPICE Model Parameters

Parameter	Units	Description
Process Parameter		
TPG	meters	Type of gate material
TOX	meters	Gate oxide thickness
LD	meters	Channel length reduction from drawn value
WD	meters	Channel width reduction from drawn value
Electrical Parameter		
UO	cm2/V.s	Zero bias low field mobility
VTO	V	Threshold voltage, long, wide device, zero substrate bias
THETA	V-1	Gate field induced mobility reduction parameter
RS	Ohm	Source series resistance
RD	Ohm	Drain series resistance
DELTA		Narrow channel effect on the threshold voltage
NSUB	cm-3	Substrate sensitivity parameter (Effective substrate doping)
XJ	m	Short channel correction to the substrate sensitivity
ETA		DIBL coefficient
KAPPA	V-1	Channel length modulation effect on the drain current
NFS	cm-2	Sub threshold region fitting parameter
CGSO	F/m	Zero bias gate-source capacitance
CGDO	F/m	Zero bias gate-drain capacitance
CGBO	F/m	Zero bias gate-bulk capacitance
XQC		Charge partitioning parameter
Additional Mobility Parameter		
BEX	V-1	Temperature effect on the low field mobility

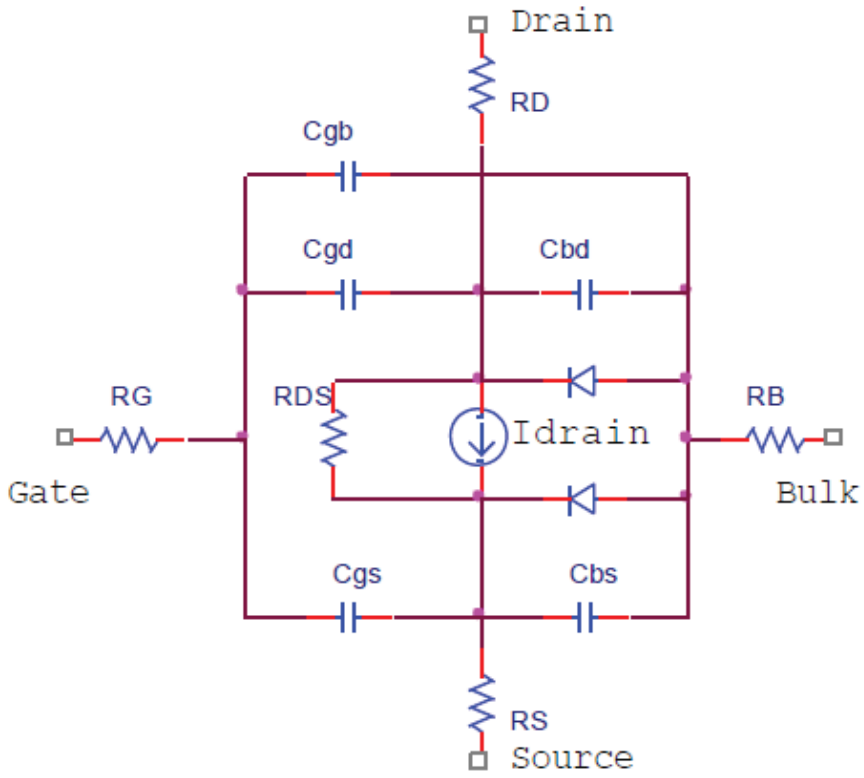

Figure 13: SPICE MOSFET schematic

The current source represents the drain current in the depletion model. Cgb, Cgd, Cbd, Cbs and Cgs are the parasitic capacitances between different terminals. The MOSFET model has intrinsic ohmic resistances in series with the drain, source, gate and substrate represented by RD, RS, RG and RB, respectively. RDS represents the shunt resistance paralleled with the drain and source.

The SPICE model of power MOSFET IRF034 is used in the entire simulation procedure. This MOSFET is used as a switch that is controlled by the Pulse Width Modulation signal that is applied to the gate terminal of this MOSFET.

The Spice model of a LEVEL - 3 IRF-034 power MOSFET is shown here

```
.model IRF034  NMOS (Level=3 Gamma=0 Delta=0 Eta=0 Theta=0
Kappa=0.2 Vmax=0 Xj=0
+          Tox=100n Uo=600 Phi=.6 Rs=31.69m Kp=21.5u W=1.3
           L=2u Vto=3.441
+          Rd=1.139m Rds=266.7K Cbd=2.857n Pb=.8 Mj=.5 Fc=.5
           Cgso=579p
+          Cgdo=456.3p Rg=8.548 Is=184.5f N=1 Tt=365n)
*          Int'l Rectifier     pid=IRFC034    case=TO3
*          88-08-25 bam   creation
```

The SPICE models that are implemented and modeled in desiging the LED driver are explained in detail in this chapter. The next chapters are dedicated to designing the drivers and modelling them for improving the efficiency.

The power MOSFET component structure is illustrated in Figure 14 [21].

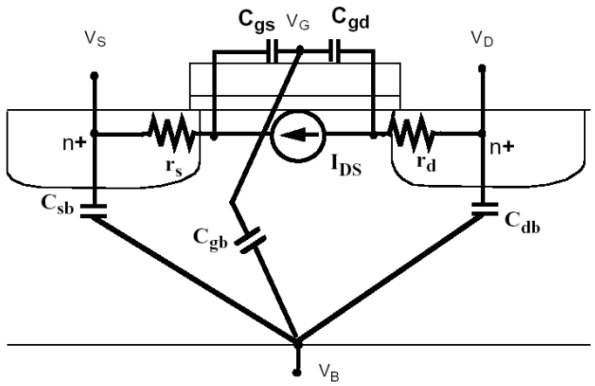

Figure 14: Power MOSFET component structure

Chapter 3

Driver Design

Background on SPICE software and modeling of circuit elements are detailed in the previous chapter. This chapter is dedicated to the design of the LED drivers and comparing the efficiencies at which these drivers operate.

3.1 Basic Driver

A very basic model for designing a driver for an LED is illustrated in Figure 15. In this model, the current through the LED is controlled by a resistor placed in series with it. Since LEDs are very sensitive to the amount of current in them, the driver should be designed very carefully and the amount of load should be taken into consideration.

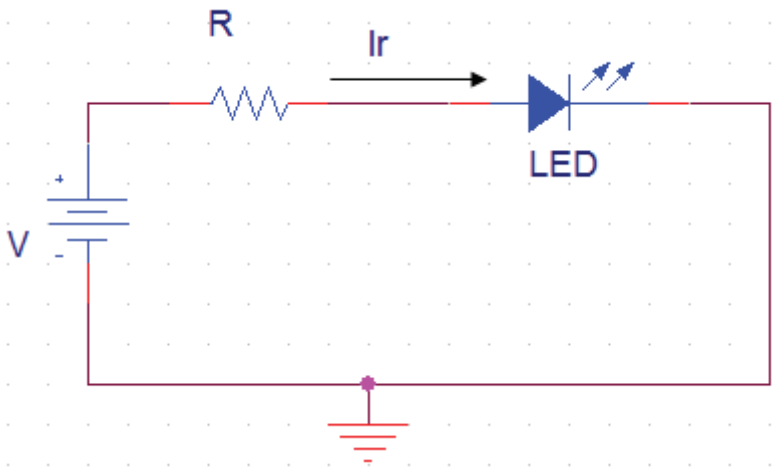

Figure 15: Basic LED driver

The resistor that is placed in series will limit the amount of current in the LED and thus save the LED from burning up. However, the main disadvantage behind this kind of operation is the power loss. In this case, most of the power is lost in the resistor.

$$P_{loss} = V_r * I_r = I_r^2 * R \quad (16)$$

As we can observe from the above equation, the value P_{loss} is directly proportional to the product of resistance and square of the current. This power loss is mainly dissipated as heat through the resistor. Although this resistor serves the purpose of limiting the amount of current entering the LED, this loss in power is highly undesirable. In some cases the power loss in the resistor is more than 75% of the actual power that is supplied to LED [22].

In order to eliminate this undesirable power loss across the current limiting resistor, an alternative driver design that eliminates this loss is considered, as illustrated in Figure 16.

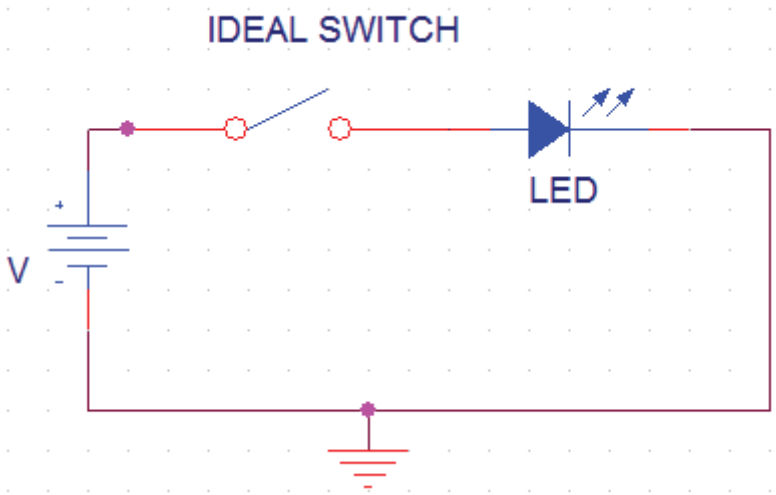

Figure 16: LED driver with ideal switch

In this design, the resistor is replaced by a switch as illustrated in Figure 16. This switch is operated by a controlling signal which alters the duty cycle. This duty cycle indeed dictates the amount of current that flows through the circuit.

In this second case:

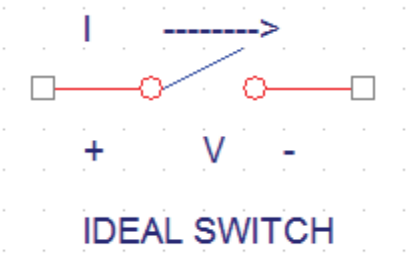

Figure 17: Operation of an ideal switch

When the switch is closed: $V = 0$

When the switch is open: $I = 0$

In either case: $P_{loss} = V * I = 0$

So, the ideal switch consumes zero power. This is the basic principle used in designing the drivers for the remainder of this thesis. A MOSFET is chosen to perform all the functions that an ideal switch can offer. An alternative to the MOSFET, the bipolar junction transistor, is avoided in order to eliminate the power processing losses that coincide with its usage. N-channel enhancement-mode power MOSFET is used in all the simulations that are performed in this thesis. N-channel enhancement-mode is widely used for power switching circuits because of its low on-state resistance compared to P-channel devices [23].

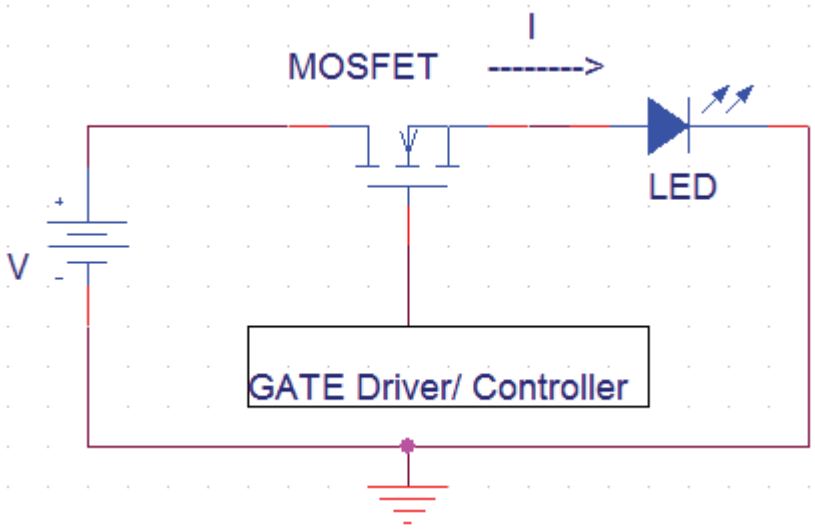

Figure 18: MOSFET replacing an ideal switch

Figure 18 helps in understanding the basic functionality of a gate operated MOSFET working as a switch. The GATE driver/ Controller controls the on-time and off-time of this MOSFET. The way this controller works is explained in more detail in the later part of this section. Also, this above circuit is a very basic schematic for a driver, a more desirable current waveform through the LED can only be accomplished by adding some passive components into the circuit without compromising on the overall efficiency.

3.1.1 MOSFET and HIGH SIDE DRIVE advantages

The advantages of using a MOSFET with a High Side Drive configuration are as follows. The on-state resistance has no theoretical limit, so the energy loss in the on-state is very low. Usage of a snubber and other techniques can be applied to reduce the losses that occur when switching without worrying about voltage or temperature-dependent switching effects in the MOSFET [24]. Short to the ground cannot destroy the load. Also, there is no load corrosion because of its connection to the ground [25].

3.2 LED Driver Designs

Based on the simple driver design illustrated in the previous section, three drivers for the LEDs are proposed. In all the three designs the pulse generator that produces the voltage pulses is identical.

3.2.1 Driver Design 1

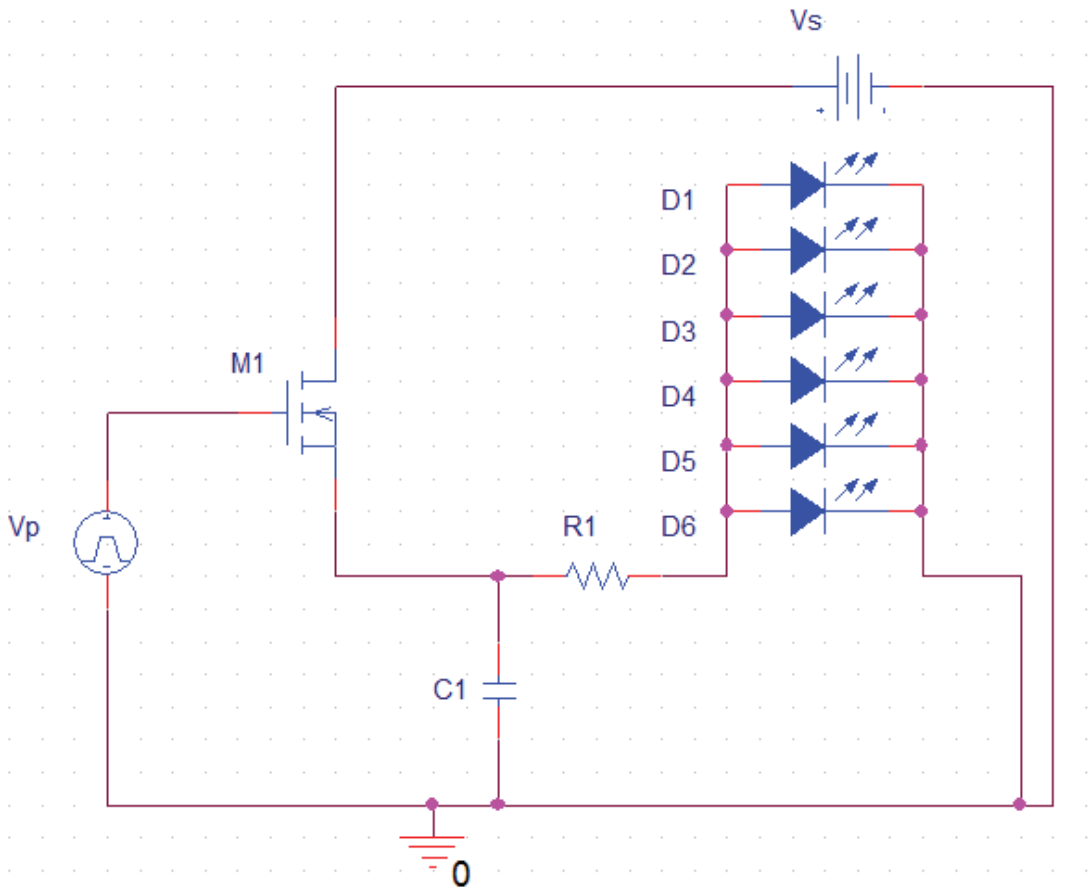

Figure 19: LED driver design 1

MOSFET M1 is controlled by a voltage pulse generator, Vp, which produces the voltage pulses with 20V as its peak voltage and 0V as its minimum voltage. The rise time TR and fall time TF are both equal to 0.05ns which has been chosen for convergence

purposes. The pulse generator Vp is operated at a frequency of 20 kHz at this stage and is generalized to a broader spectrum at later stages. The simulation is run for 1ms collecting the data points at a step size of 0.01μs.

To accomplish a duty cycle of 50% out of this pulse generator the expressions of the pulse width (PW) and period (PER) are modified as following:

$$PW = \frac{0.5}{FRQ} \tag{17}$$

$$PER = \frac{1}{FRQ} \tag{18}$$

where,

FRQ is the frequency at which the pulse generator is operated. This FRQ can be easily changed by using the "PARAMETERS" command in the SPICE software. Since, frequency is inversely proportional to the pulse width; the circuit can be operated by changing the duty cycle through which we can achieve the dimming phenomenon.

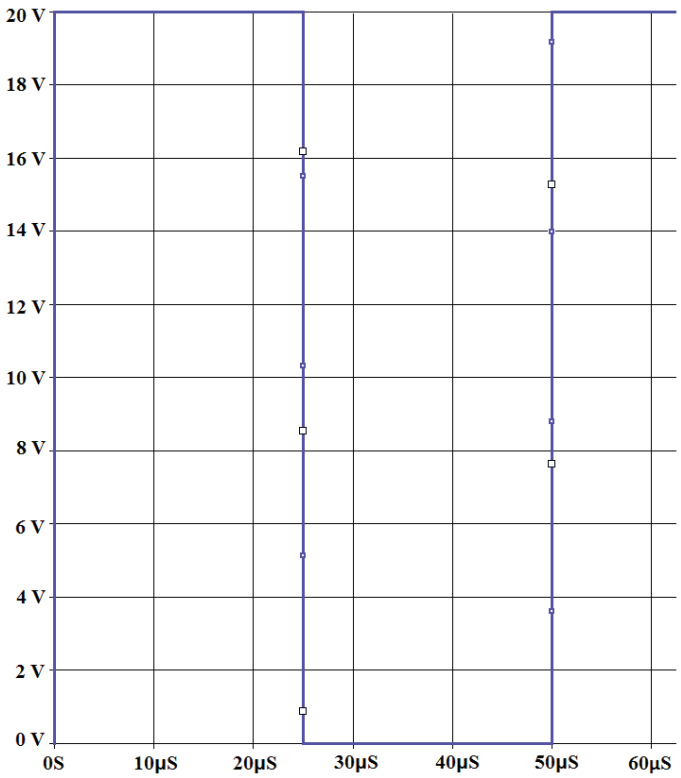

Figure 20: Output of pulse generator (Vp)

The waveform that is produced by the pulse generator (Vp) is shown in Figure 20 oscillating between 0 to 20V with 50% duty cycle. The pulses generated by Vp indeed control the ON and OFF cycles of the MOSFET M1. The voltage probe at the source terminal of the MOSFET M1 is plotted in Figure 21.

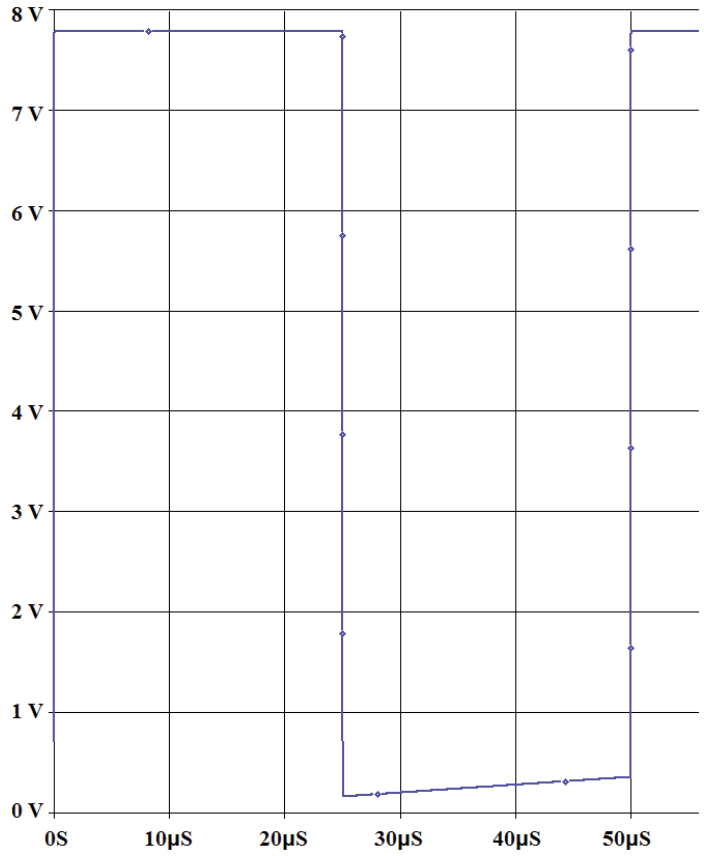

Figure 21: Voltage output at source terminal of MOSFET M1

Here, the source voltage Vs = 8V. When M1 is turned on by the positive pulse Vp, the M1 looks like a closed switch, which lets current flow through the MOSFET and the LEDs in the first half cycle between 0-25µs. In the next half cycle the circuit is open and hence there is no current flow in either of them. This describes the influence of the pulse generator on the driver output.

The current measured at the source terminal of the MOSFET generates the following waveform which is illustrated in Figure 22.

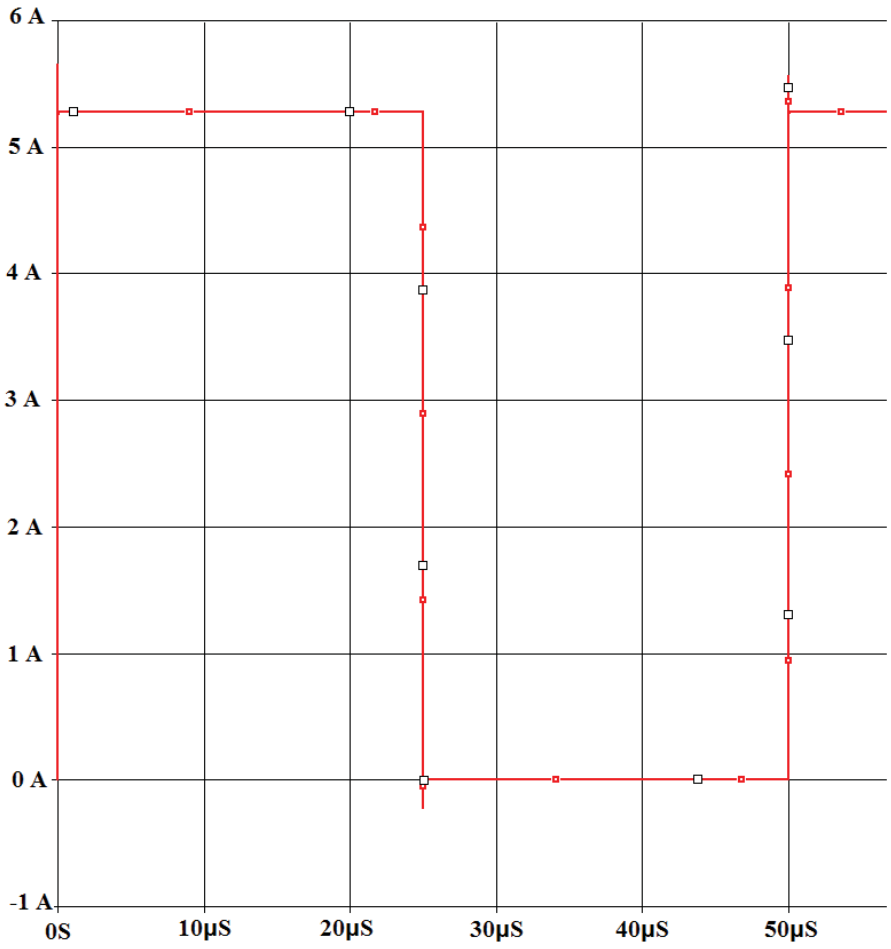

Figure 22: Current output at source terminal of MOSFET M1

Here, the peak current that is flowing through the MOSFET in the ON state is 5.27 A . The spikes caused by switching are produced by parasitic elements like stray inductances, which naturally exist in series and parasitic capacitances which exist in parallel. These parasitic elements produce voltage and current spikes when changes in current or voltage are exposed to them [26]. The soultion for reducing/eliminating these spikes are discussed in detail in the chapter 4. Resistor R1 controls the current that is enterning the LEDs, and the capacitor C1(1nF) filters most of the AC components and the spikes that are entering the LEDs.

3.2.2 Driver Design 2

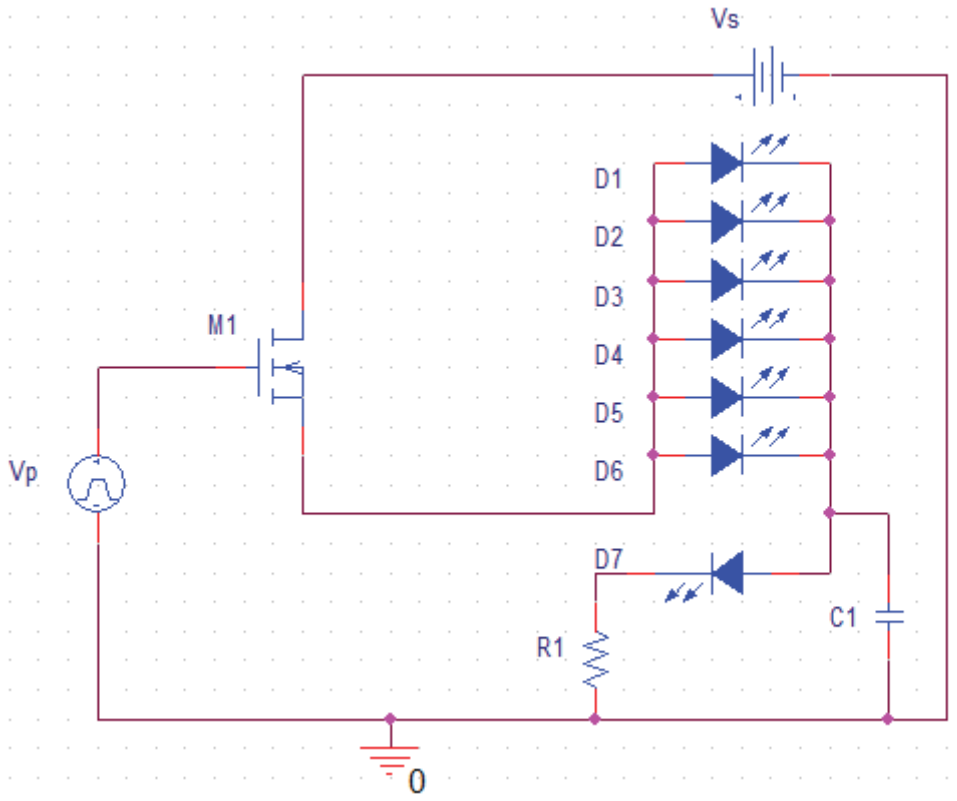

Figure 23: LED driver design 2

In this second design, the voltage pulse generator Vp is operated at the same frequency of 20 kHz with a 50% duty cycle similar to that of circuit 1. The voltage source Vs is still the same and equal to 8V. This operation procedure of this circuit is very similar to that of the earlier design, but there are a few modifications in the configuration of the circuit elements.

In order to provide a low impedance path to the high frequency switching noise, a capacitor C1 is placed across the LEDs. The position of the resistor R1 is shifted, and it acts as a current limiter for the LEDs. An additional LED is added to the second design with the goal of increasing the efficiency of operation.

Voltage output at the source terminal of the MOSFET is plotted in Figure 24. The process of operation is the same as the above circuit. When the MOSFET is in the ON state the voltage source Vs is in a closed circuit with the LEDs. The peak of the waveform must ideally equal to 8V, but there is a slight voltage difference from the predicted waveform. This small voltage drop of 85.5mV across the MOSFET M1 is caused by the small resistance between the gate and the source terminal of the LEVEL-3 SPICE model of the MOSFET M1 (IRF034).

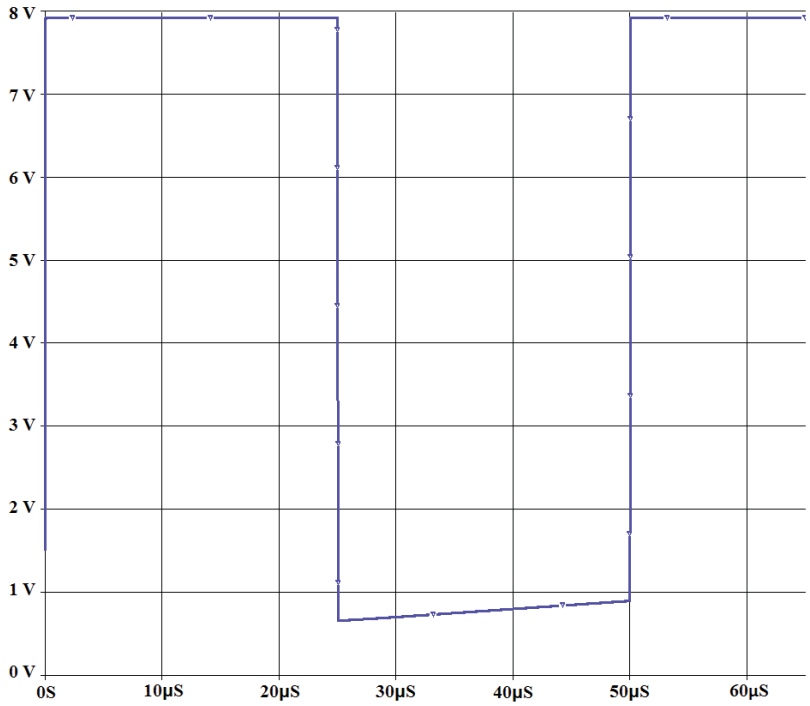

Figure 24: Voltage output at source terminal of MOSFET M1

The current waveform through the MOSFET source is illustrated in Figure 25. As stated in the earlier design, the spikes that are caused by the parasitic elements like capacitors and inductors will be eliminated by using a snubber circuit, which will be covered in the next chapter.

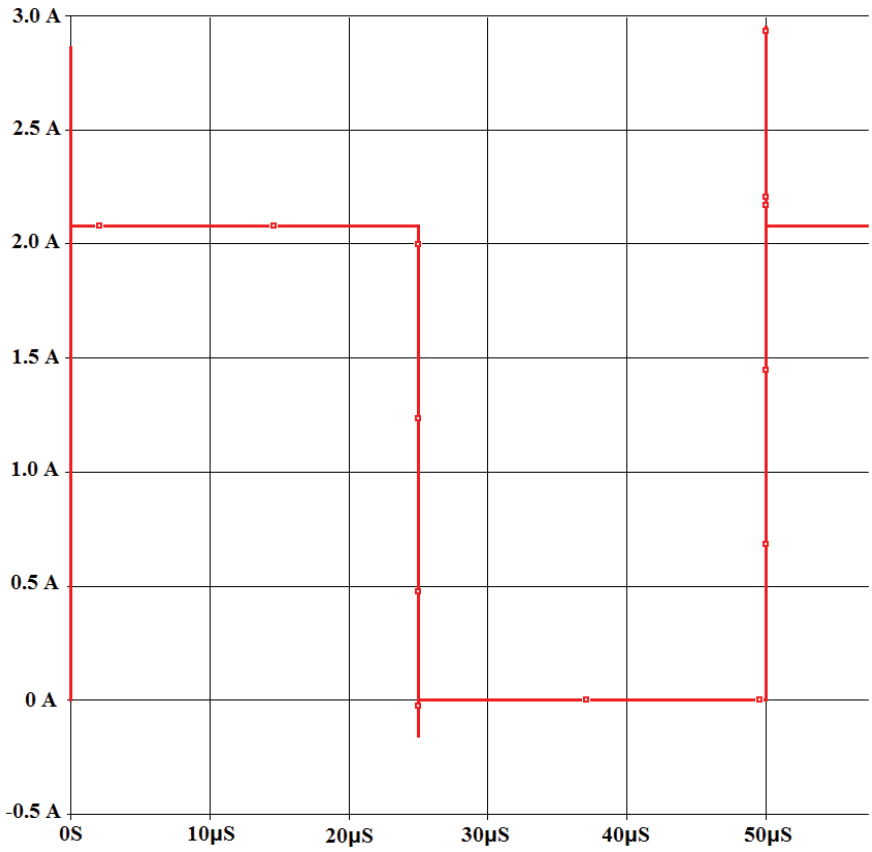

Figure 25: Current output at source terminal of MOSFET M1

3.2.3 Driver Design 3

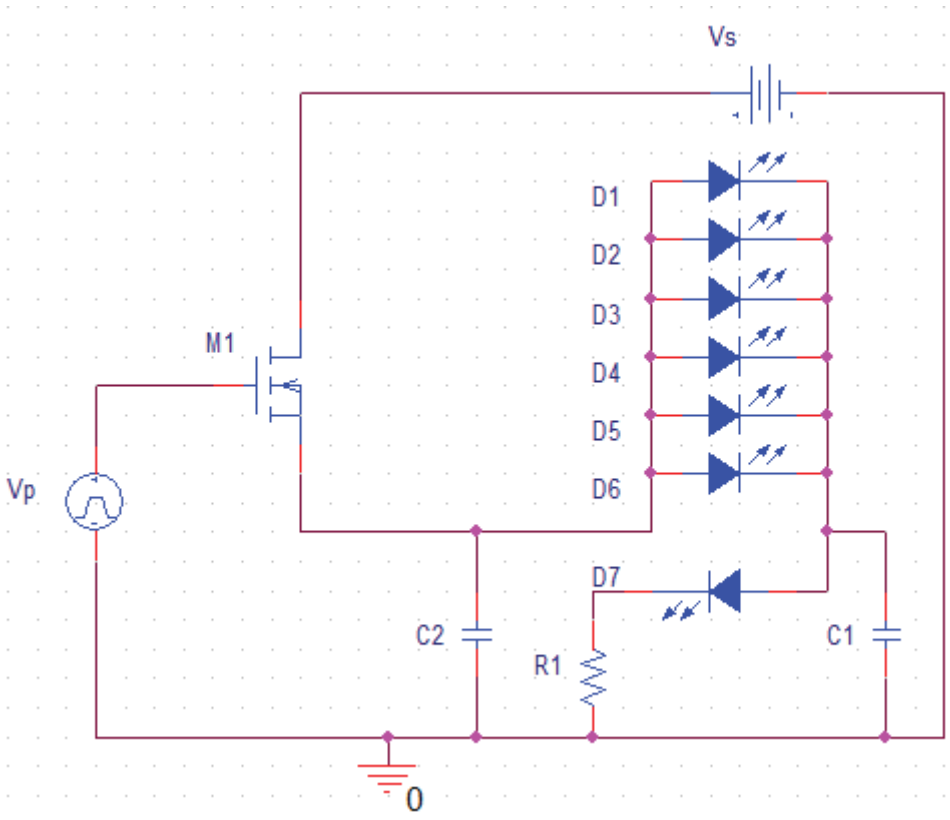

Figure 26: LED driver design 3

In a goal to reduce the high frequency switching noise entering into LEDs, the capacitor C2 is placed in parallel. The frequency of operation, duty cycle, and the rest of the circuit elements remain unchanged.

The current waveforms of the MOSFET source and the individual LED are plotted in Figures 27 and 28. Figure 27 illustrates the current that is leaving the source terminal of the MOSFET M1 and has a stable current value of 2.07A, but value of the spike is close to 113.7 A . As stated earlier, these huge spikes are caused by the parasitic circuit elements. The voltage waveform is nearly identical to that of the Driver Design 2, which is illustrated in Figure 24. The current that is entering the LEDs is spike free

because of the capacitor C2, as observed in Figure 28. Note that the current is high when the MOSFET is switched on indicating that the LEDs are consuming power. The turn-off time is increased due the discharge of the capacitance C2 through resistor R1. The turn-on time is not affected by the capacitance C2 because there is no current limiting element.

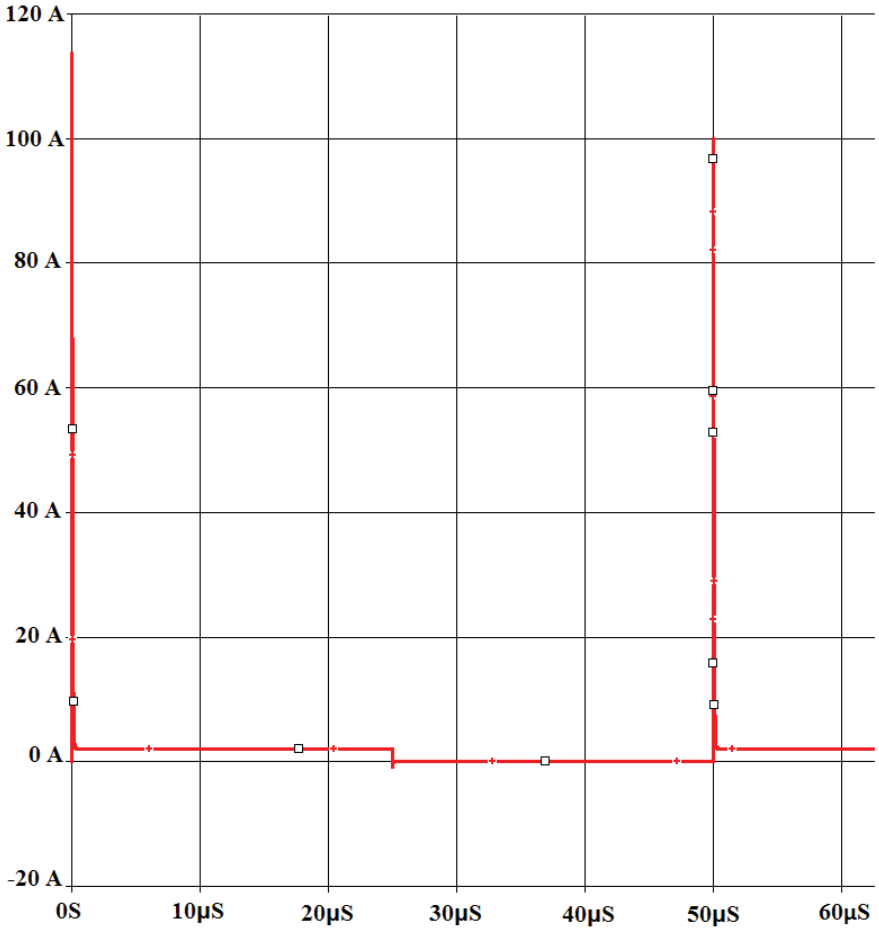

Figure 27: Huge current spikes at source terminal of MOSFET M1

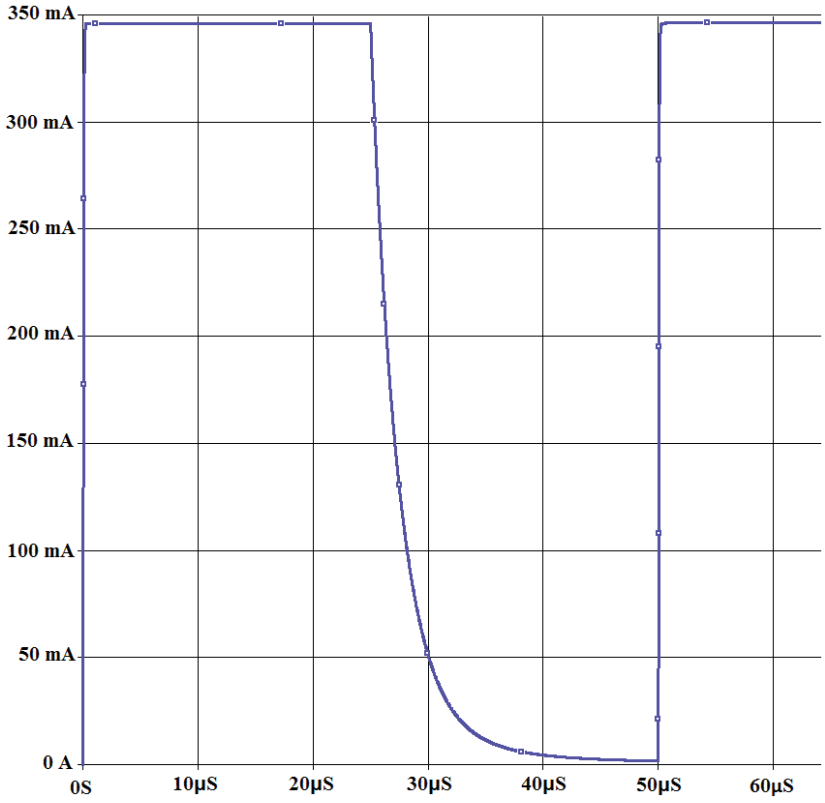

Figure 28: Current with no spikes entering LEDs

3.3 Efficiency Calculation

This section gives a brief understanding of the methods that are used for the efficiency calculation and compare the efficiency of the three driver circuits.

The efficiency is calculated as the ratio of the output to the input power.

$$Efficiency = \frac{Useful\ output\ power}{Total\ input\ Power} = \eta \tag{19}$$

There are many methods for performing the discrete integration required to calculate the efficiency of the above circuit such as Fourier series, Simpson's rule, and Trapezoidal rule. The Trapezoidal rule was chosen to perform this task because of its

accuracy when periodic functions are integrated over their period [27] [28] and the ease of applying the above rule on the data that was exported from the obtained waveform.

The trapezoidal rule works by breaking the interval $[a, b]$ to "n" subintervals and then approximating the region under the graph [29] by trapezoids as shown in Figure 29.

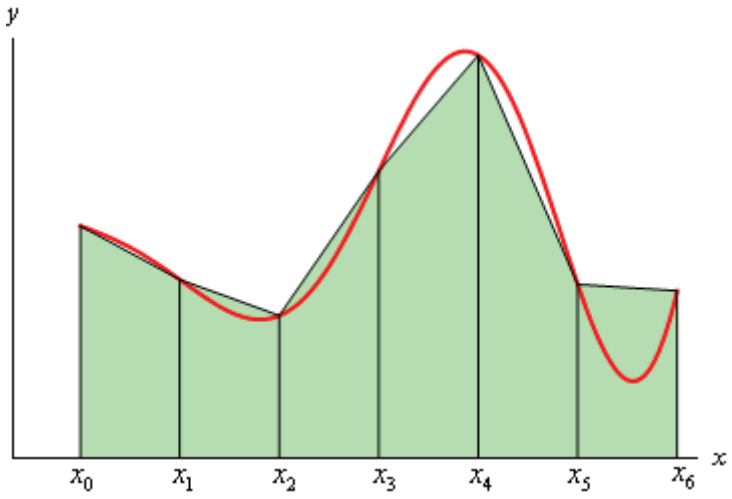

Figure 29: Trapezoid approximation of sub intervals

The generalized formula of the trapezoidal rule is given by

$$\int_a^b f(x)\,dx \approx (\frac{\Delta x}{2})[f(x_0) + 2f(x_1) + 2f(x_2) + \cdots + 2f(x_{n-1}) + f(x_n)] \tag{20}$$

where,

$$\Delta x = \frac{b-a}{n} \tag{21}$$

The power dissipation / consumption graph obtained by placing a probe on a component is exported to a ".CSV" file for all the data points that are simulated in the experiment. The above formula was applied on all of the individual data points that were obtained from the waveform to calculate their individual power dissipation /

consumption. After obtaining these values, efficiency is computed from the ratio of the total output power to the total input power.

Efficiency comparisons and their individual circuit parameters are tabulated in the Table 3.

Table 3: Efficiency comparison of LED driver circuits

Parameters	Circuit 1	Circuit 2	Circuit 3	Unit
Frequency Operated	20000	20000	20000	**Hz**
Pulse Width	2.50E-02	2.50E-02	2.50E-02	**mSec**
Period	5.00E-02	5.00E-02	5.00E-02	**mSec**
Duty Cycle	50%	50%	50%	**Percent (%)**
Gate Pulse Voltage(Vp)	20	20	20	**Volts**
Resistance	1	1	1	Ω
Capacitances	1n	1n	C4=1u,C1=1n	**F**
Source Voltage(Vs)	8	8	8	**Volts**
Simulation Profile	0-1ms,0.01us	0-1ms,0.01us	0-1ms,0.01us	**Runtime, Step size**
Total Efficiency	31.35%	72.95%	71.13%	

Although all the three circuits are supplied with the same amount of power, all three have different efficiency values because of the circuit arrangement and placement of the circuit elements.

3.4 Spike problems and efficiency errors

The spikes / ringing at the terminals of the MOSFET that are observed in the earlier figures are a major problem. The parasitic capacitance and inductance that is present on the leads create an LCR circuit which can destroy the MOSFET in real-world conditions.

Efficiency calculations from the data points that are collected from the SPICE simulation will lead to a value with some error, because SPICE considers the spikes as real power. Although this error is a considerably small value, it might affect the total value in longer run periods.

In order to eliminate the spikes/ ringing in the circuit, individual snubber circuits are designed for these three driver circuits. These will be explained in the next chapter.

Chapter 4

Snubber Design and Diode Modeling

The spikes / ringing that occurred across the MOSFET in the earlier design are resolved in this chapter by designing a snubber circuit. Also, the different waveforms after using a snubber circuit are illustrated. The later part of this chapter deals with the modeling and arrangement of the LEDs to improve the overall driver efficiency.

4.1 Need for snubber circuit

Power MOSFETS are the switching devices that are used universally in most power electronic circuits. Overheating, extreme changes in current and voltage, EMI noises and switching losses are the leading problems that any switching devices encounter.

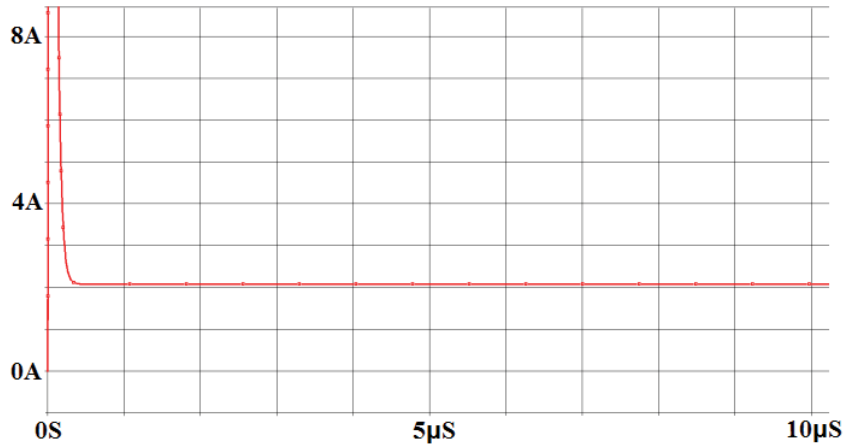

Figure 30: Transient current spike

Figure 30 shows that these extreme spikes which we are concerned about occur for much shorter periods than the actual switching periods. In order to explain the cause of this ringing in general a model circuit illustrated in Figure 31 is considered and described in detail.

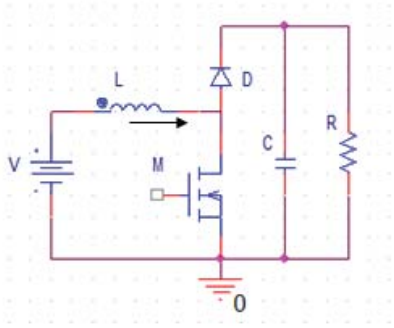

Figure 31: Model switching circuit

From Figure 30, in normal operation the output voltage/current stays constant for the majority of the switching period. Therefore, in the above circuit, load R and capacitor C can be substituted with a voltage source for sake of simplicity. Similarly the inductor can be replaced by a current source. The modified circuit is illustrated in Figure 32.

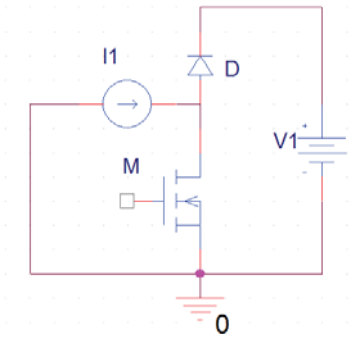

Figure 32: Simplified circuit

Here the MOSFET M acts as a switch that is controlled by a voltage pulse which is not shown in the above figures. When the switch is open, current flows through the

diode D into V1. When the switch changes to a closed state, the current flowing through the MOSFET steadily increases. However, as long as the current in the diode still has some positive value the voltage across the switch stays at V1. The value of the voltage V1 falls once the current flowing through the diode reaches zero. As the switch turns into the off state, the voltage across the terminals starts rising. However, the current will not fall until the voltage reaches V1 because the diode D stays in the reverse biased stage as illustrated in Figure 33.

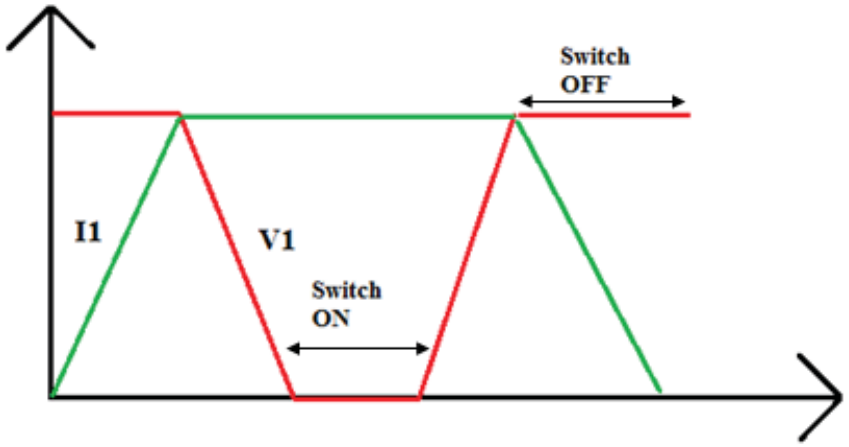

Figure 33: Voltage (V1) and Current (I1) switching cycle

The above mentioned process is referred to as Hard-Switching. This phenomenon of supporting the peak current and peak voltage concurrently exposes the switch to high stress [30], which leads to very high switching losses. In real-world the parasitic elements such as stray inductance (due to finite size of the circuit) and inherent capacitances make this stress even worse. These parasitic elements are inevitable in all switching elements.

Snubber circuits are required to limit or eliminate these extreme changes in current and voltage during turn-on and turn-off processes.

4.2 Types of snubber circuits

There are many types of Snubber circuits available depending upon their application. The types of snubbers also vary depending on the power supply circuits [31] (i.e., DC-DC or AC-DC etc.).

Some of the basic snubber circuits are:

1. RC snubber circuit
2. RCD snubber circuit
3. Turn-off snubber circuit
4. Turn-on snubber circuit

Although there are many other variations of snubber circuits the above stated configurations are the basis for all other designs. Snubber circuits are even categorized depending on the type of transistor that is to be protected (i.e., BJT, MOSFET or IGBT). The necessity and the design of the turn-on snubbers for the driver circuits are discussed in this thesis.

4.3 Turn-on snubber circuit

The huge spikes that are caused when switching the MOSFET to the ON state as shown in Figure 30 can be eliminated / limited by using the turn-on snubber circuit shown in Figure 34. Here, the series connection of the diode D and resistor R_S is placed in parallel with the inductor L. Gate resistance R_g also helps to control the spikes.

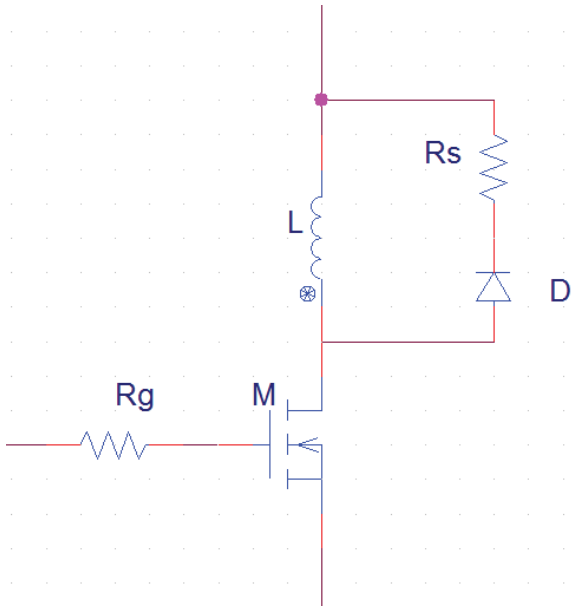

Figure 34: Turn-on snubber protecting MOSFET M

During the turn-On cycle the inductor L controls the huge inrush current (Ip) flowing into the parasitic capacitance in the MOSFET. When the MOSFET turns off, the energy which was stored earlier in the snubber inductor will be dissipated through the snubber resistor R_S. Inserting a series gate resistance R_g reduces the current spikes by changing the charging and discharging cycles of the parasitic capacitances C_{GS} and C_{GD} in the MOSFET.

The energy stored in the inductor is given by

$$E_L = \frac{L * I_p^2}{2} \tag{22}$$

where,

L = Inductance in Henries

I_p = Current through the inductor

The time taken by an inductor to reach its steady state is given by the time constant τ as:

$$\tau = \frac{L}{R} \tag{23}$$

where,

L= Inductance in Henries

R= Resistance in Ohms (Ω)

The inductor by its nature opposes the change of electric current through it [32]. In the above snubber circuit, the inductor is chosen such that the time constant is close to the period of the spike which is much smaller than the switching period. Not only the rise time but also the dissipation across the resistor R_S increases as the inductor is made large. There is a tradeoff between switching loss, dissipation, and rise time. This method used by the turn-on snubber will eliminate the current spikes.

4.4 Turn-on snubber with the Driver Circuits

The Driver circuits that were designed in the previous chapter are modified by inserting a turn-on snubber circuit. The test values and the waveforms that are obtained after repeating the experiment are discussed in this section.

4.4.1 Driver Design 1 with the snubber

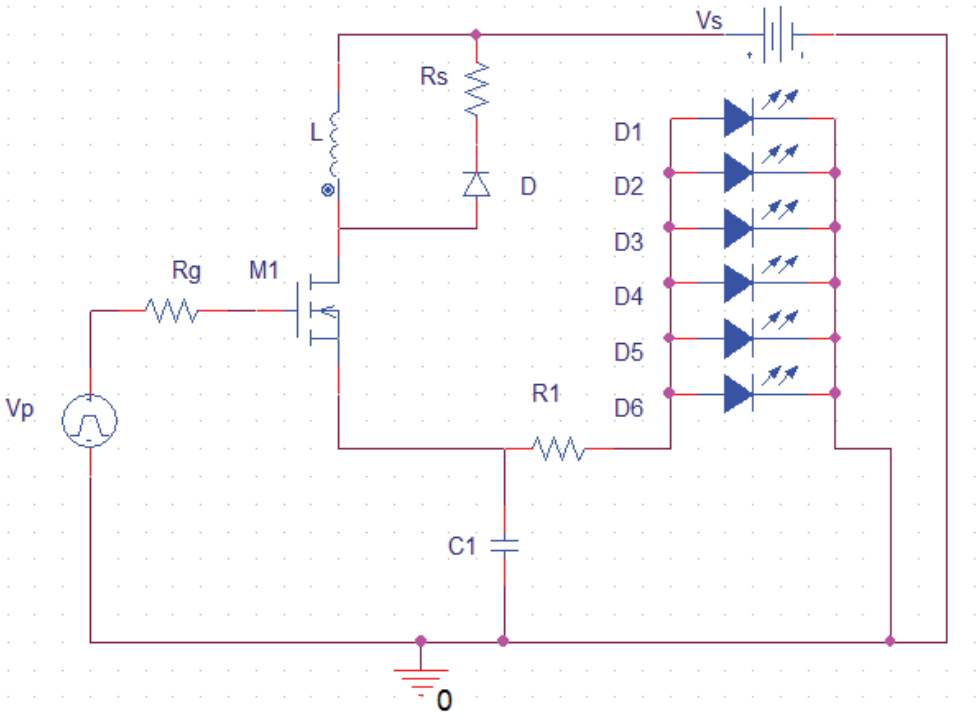

Figure 35: LED driver design 1 with turn-on snubber

The operation of the above circuit remains exactly the same as explained in the previous chapter except for the addition of the snubber circuit. The MOSFET M1 which is controlled by the Pulse generator Vp, is again operated at the same frequency of 20 kHz with a duty cycle of 50%.

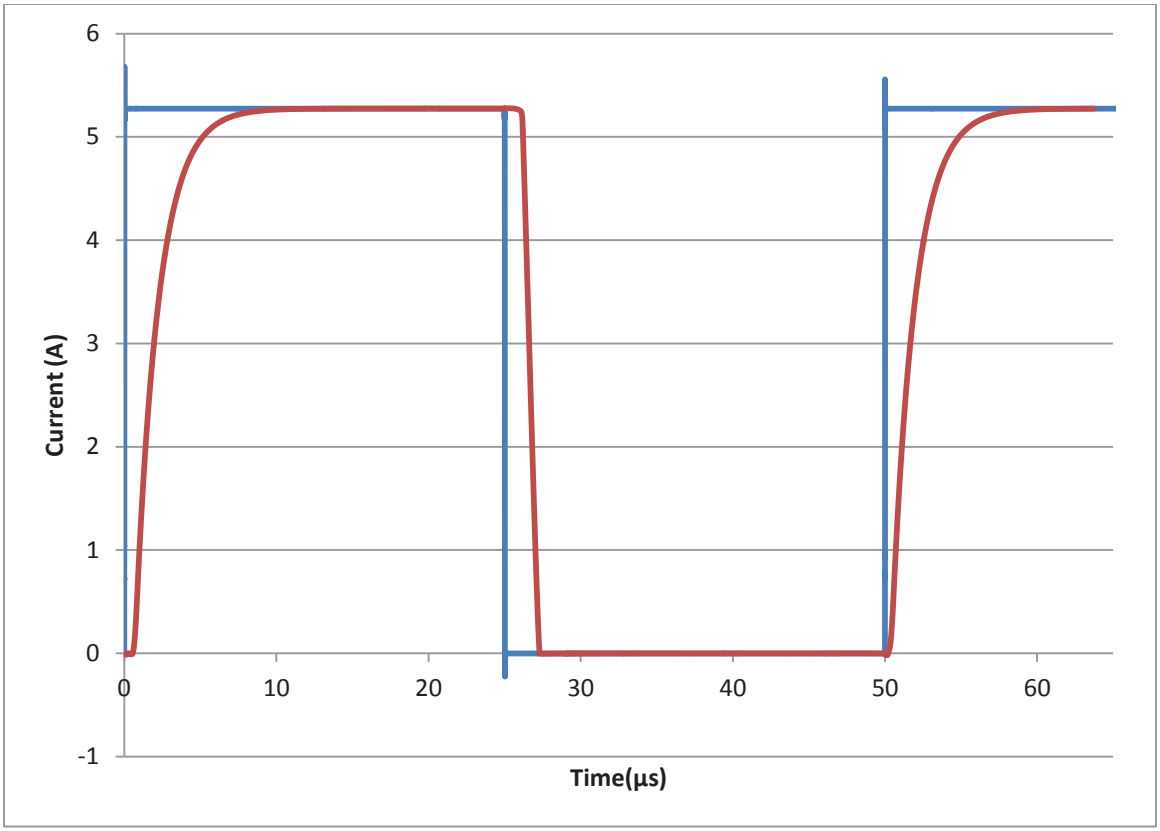

Figure 36: Current output at source terminal of MOSFET M1

The waveforms in Figure 36 are the current flowing through the MOSFET before and after integrating the snubber circuit into the driver circuit. As we can observe from the waveforms in Figure 36, the spikes are eliminated when compared to that of the earlier waveform in Figure 22.

The rise time of the later waveform (i.e., with snubber) has a value close to 4.14µs compared to the very low rise time of 0.01 µs for the same circuit without snubber.

Although there is a time delay that is obvious from Figure 36, it is understandable that there is a tradeoff between the switching loss and the delay time as mentioned earlier.

4.4.2 Driver Design 2 with the snubber

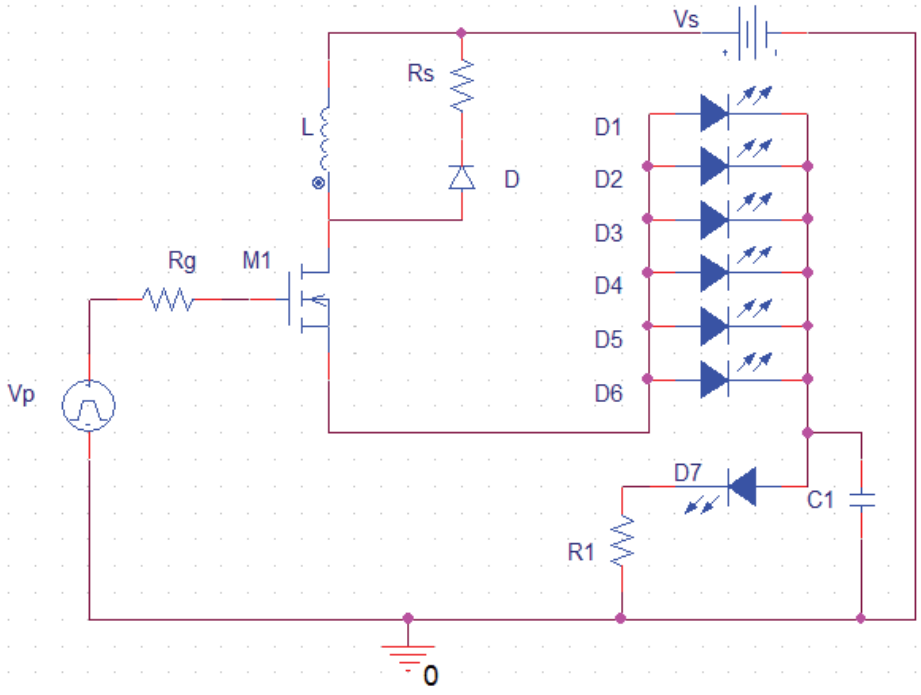

Figure 37: LED driver design 2 with turn-on snubber

The Driver Circuit that was designed in the earlier chapter is modified by adding a snubber circuit, illustrated in Figure 37. The basic functionality of the above circuit is same as the one explained in the earlier chapter.

The waveforms obtained by placing a current probe at the source terminals of the MOSFET without the snubber circuit and with snubber are illustrated in Figure 38. The spikes that occurred in the earlier simulation (Figure 25) are completely eliminated after plugging the snubber into the circuit. By taking the data points from the below plotted graph the accuracy of the measured efficiency increases as the ringing is no longer considered as power dissipated / absorbed.

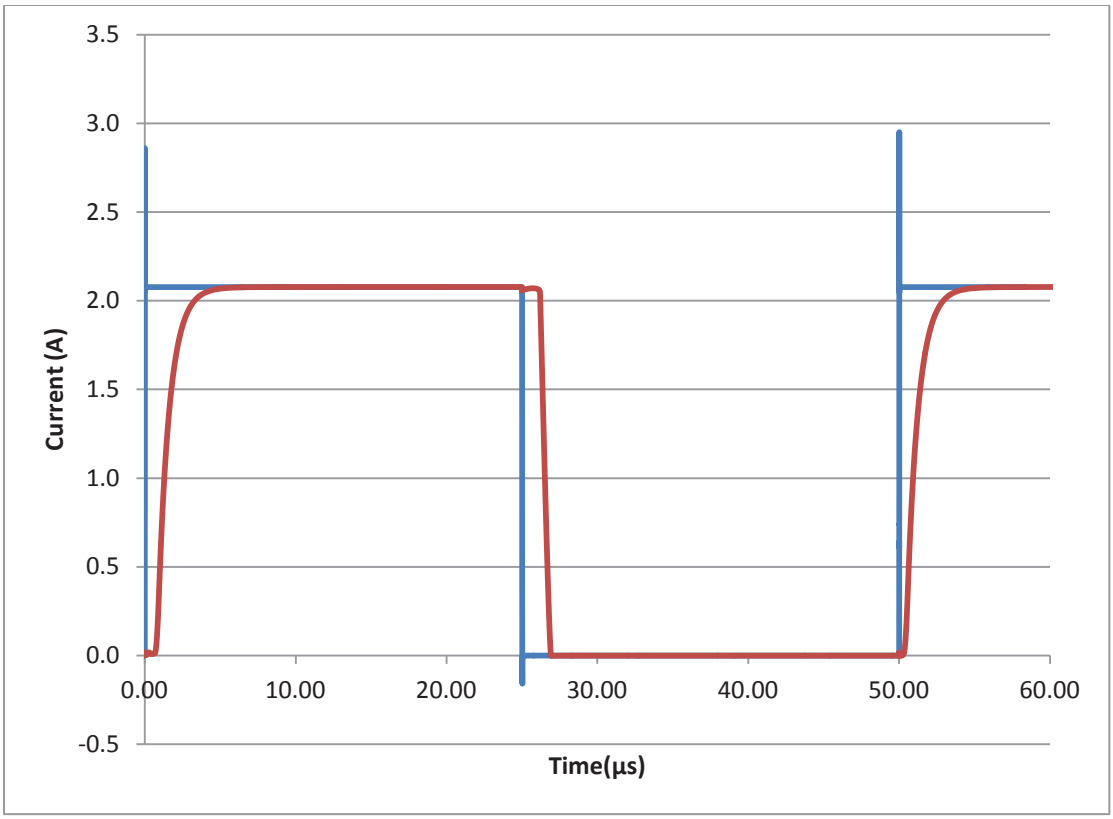

Figure 38: Current output at source terminal of MOSFET M1

The rise time of the later waveform (i.e., with snubber) has a value close to 5.08 µs compared to the very low rise time of 0.01 µs for the same circuit without snubber.

Although there is a time delay that is obvious from Figure 38, it is understandable that there is a tradeoff between the switching loss and the delay time as mentioned earlier.

4.4.3 Driver Design 3 with the snubber

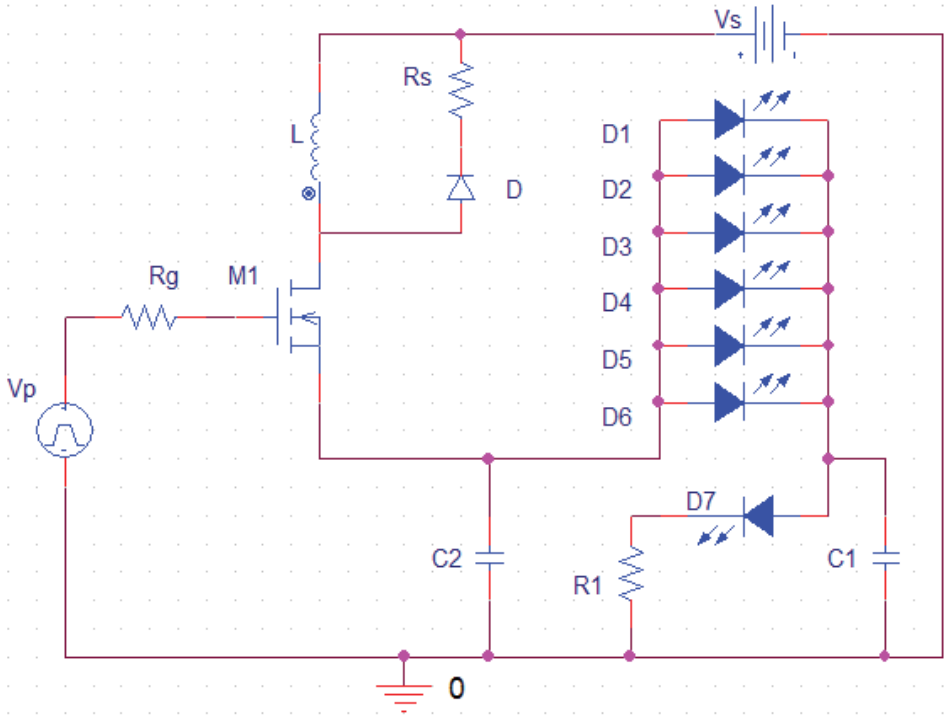

Figure 39: LED driver design 3 with turn-on snubber

Driver design 3 with the added snubber generates the waveform that is plotted in Figure 40. When observing this new generated waveform it is obvious that all of the spikes have been eliminated after adding the snubber to the circuit.

The waveforms in Figure 40 are the current flowing through the MOSFET before and after plugging the snubber circuit into the driver circuit. Huge current spike values that are close to 113.7 A (Figure 27) are eliminated here after plugging the snubber circuit into the driver circuit.

The rise time of the later waveform (i.e., with snubber) has a value close to 6.6 µs compared to the rise time <0.01 µs for the same circuit without snubber.

Although there is a time delay that is obvious from Figure 40, it is understandable that there is a tradeoff between the switching loss and the delay time as mentioned earlier. In the Figure 40, the Y-axis is scaled to a maximum value of 10 A, so that the both waveforms can be illustrated clearly on the same time axis.

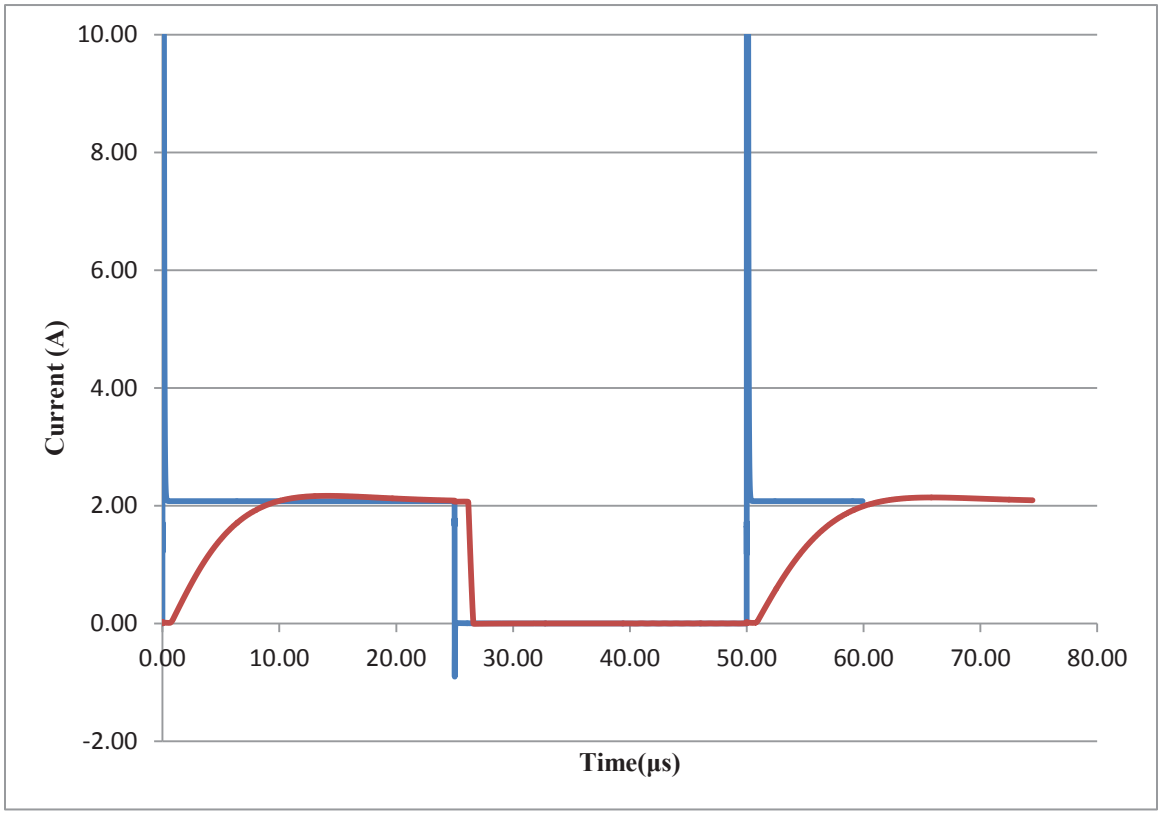

Figure 40: Current output at source terminal of MOSFET M1

When comparing the waveforms in Figure 38 and Figure 40, it is noticeable that the latter one has the larger rise time and also the overshoot is better suppressed in the earlier circuit.

4.5 Efficiency table with the snubber circuit

Table 4 gives the efficiency values obtained from the driver circuits after plugging in the snubber circuit. All of the parameters which are considered in the earlier experiment remain the same as those of Table 3. The efficiency of the circuits with the snubber is slightly reduced compared to the efficiency of the circuits without the snubber. This is due to the resistive losses in the resistor Rs and also the inductor itself. The efficiency values that are obtained with the snubber circuit are more accurate than the earlier calculations as the area under the spikes is not included in calculating the efficiency anymore.

Table 4: Efficiency comparison of LED drivers with snubber circuit

Parameters	Circuit 1	Circuit 2	Circuit 3	Unit
Frequency Operated	20000	20000	20000	**Hz**
Duty Cycle	50%	50%	50%	**Percent (%)**
Resistance	1	1	1	**Ω**
Capacitances	1n	1n	C4=1u,C1=1n	**F**
Source Voltage(Vs)	8	8	8	**Volts**
Simulation Profile	0-1ms,0.01us	0-1ms,0.01us	0-1ms,0.01us	**Runtime, Step size**
Total Efficiency(η)	31%	71%	68%	

In an attempt to increase the efficiency of the designed driver circuit the LEDs that are utilized in this design are modeled using the PSpice model editor which will be discussed in the next section.

4.6 Modeling LED to increase driver efficiency

This section is mostly dedicated to modeling the LED parameters which were detailed in the chapter 2 of this thesis. Circuit 2 is considered in this stage of study because of its higher efficiency and decent waveform.

Cadence - OrCAD PSpice offers a tool called PSpice model editor, which allows us to model any SPICE model available in the directory. This tool is very helpful for modeling a LED based on basic diode principles and also to model the design which reflects the commercial LED models that are available in the market.

Parameters that are used for the LED modeling in our case are:

- Emission coefficient N
- Ohmic resistance Rs
- Saturation current Is
- Zero-bias junction capacitance CJO

4.6.1 Modeling Default Diode Model

```
.MODEL MLED81 D
+ IS=10.000E-9
+ N=1.1248
+ RS=1.2366
+ IKF=45.752E-15
+ CJO=25.000E-12
+ M=.3333
+ VJ=.75
+ ISR=10.010E-21
+ BV=5.4169
+ IBV=10
+ TT=5.0000E-9
```

The above default diode model is modeled by varying the parameters that are mentioned earlier.

From Equation 4, it is obvious that the LED forward current is directly proportional to the saturation current Is. By influencing the Is value the total forward current can be managed effectively. Also, the emission coefficient N value has its influence on the forward current from the same equation.

Simulations are run by altering the different parameters from the diode model and its influence on the overall efficiency is noted. From all these experimental results a diode model is chosen which has a very high performance and also satisfies the commercial LED standards.

Below is the modified LED model after performing many simulations:

```
.MODEL MLED81 D
+ IS=10.000E-12
+ N=2.1248
+ RS=4.2366
+ IKF=45.752E-15
+ CJO=25.000E-12
+ M=.3333
+ VJ=.75
+ ISR=10.010E-21
+ BV=5.4169
+ IBV=10
+ TT=5.0000E-9
```

4.6.2 Efficiency from diode modeling

The different efficiency values that are obtained during the LED modeling are plotted in Figure 41. The horizontal axis in the graph shows the different stages of driver circuit development, starting without the snubber circuit, with snubber circuit and finally the modeled driver circuit.

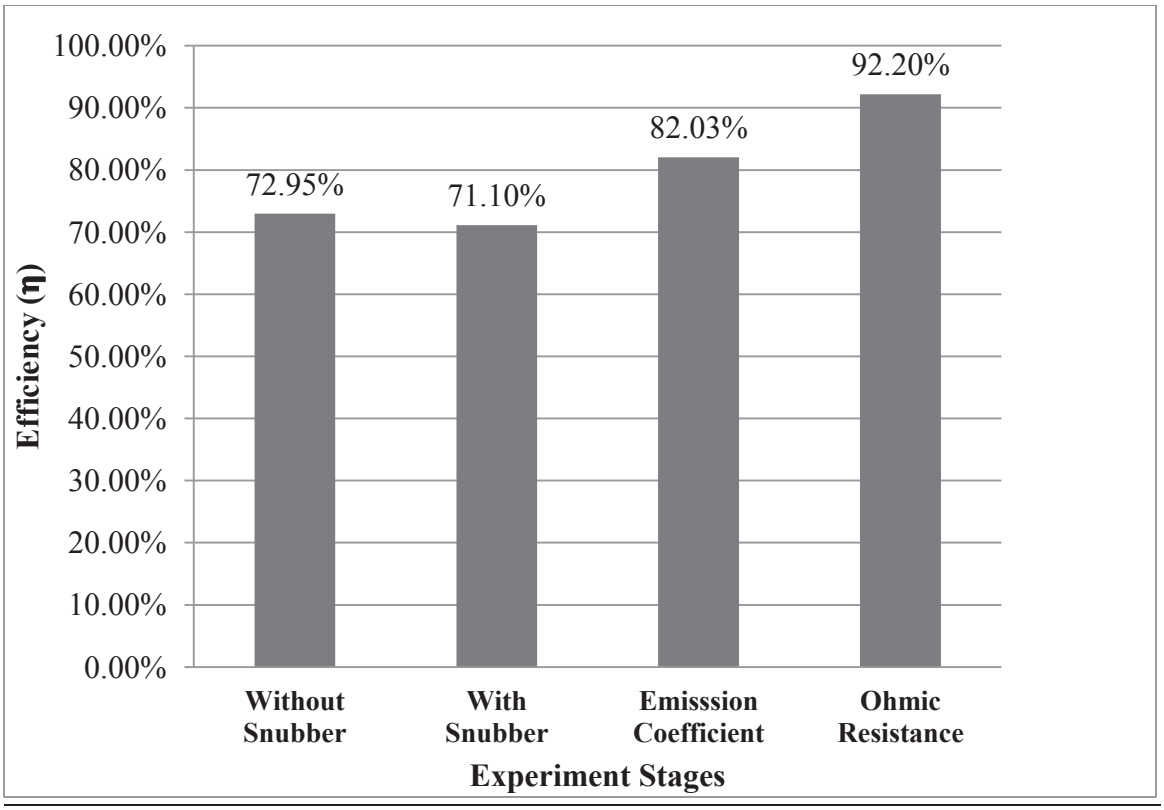

Figure 41: Efficiency graph at different experiment stages

The efficiency decreased from 72.95% to 71.10% upon adding the snubber to the circuit. This small loss was explained in the section 4.5. The efficiency increased from 71.1% to 82.03% after modeling the LEDs Emission coefficient. In order to increase the efficiency further, Ohmic resistance of the LED is modeled resulting a value of 92.2%. By adjusting the LED layout, the above efficiency values can be further increased.

4.7 Efficiency results from the commercial LED model

In the interest of comparing the above LED model with the real world available LED commercial model, the modeled LED is replaced with an OSLON LA H9GP model manufactured by the OSRAM Opto Semiconductors.

4.7.1 OSRAM commercial LED model:

```
**********************************
.MODEL LA_H9GP-9c-max_T D
+ IS=271.64E-21
+ N=2.1719
+ RS=.8785
+ EG=2.7500
+ XTI=3
+ IKF=45.752E-15
+ CJO=245.000E-12
+ M=.3333
+ VJ=.75
+ ISR=10.010E-21
+ BV=5.4169
+ IBV=10
+ TT=5.0000E-9
```

The commercial LED model LA H9GP is given above. This model is obtained from the manufacturer's PSpice library.

These OSLON families are developed particularly for the applications requiring maximum luminous flux when little consumption of space and longer lifetimes are expected [33]. These come with highly efficient semiconductor chips that use the thin-film technology. Many of these can be combined without worrying about the space because of its compact size. These products comply with RoHS specifications and do not contain any lead or other hazardous substances. These have a good thermal conductivity and also enable thermal connection to the printed circuit board. The ceramic base used in this OSLON group has the significant advantage of stable degradation characteristics in

regard to light, regardless of the wavelength. The typical lifetime of these LED are up to 100,000 hours (i.e., Continuous operation of Eleven and a half years).

The driver circuit 2 with the commercial OSLON LEDs is illustrated in Figure 43.

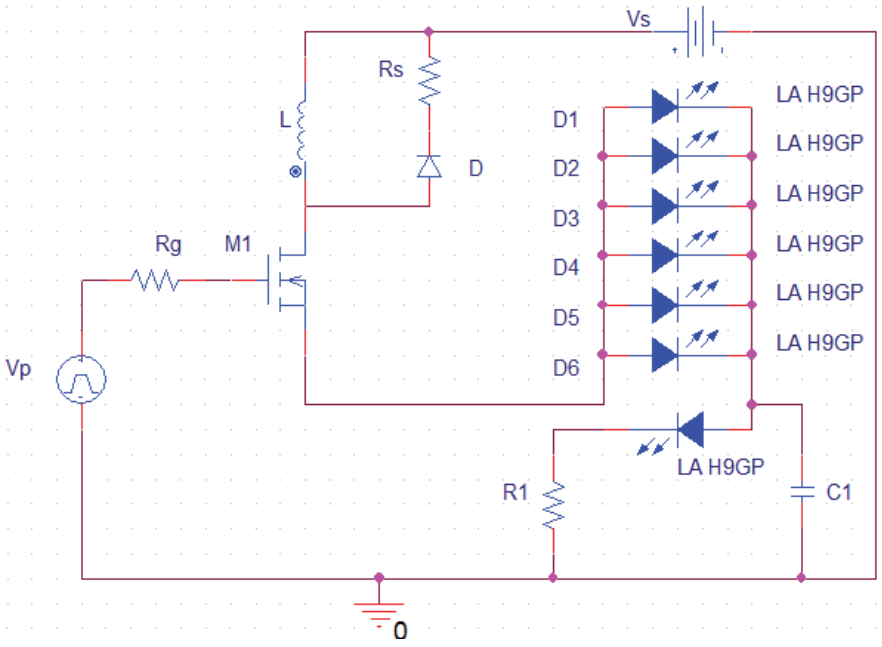

Figure 422: Driver Circuit 2 modeling OSLON LA H9GP

An efficiency of 88% is obtained when the above circuit is simulated at Vs=6V and their corresponding dissipation values are evaluated using the same method used earlier. This is slightly reduced from the estimated value of 92.20% that was calculated earlier with the more general model; however this new calculation is probably more accurate because we are using a more advanced model.

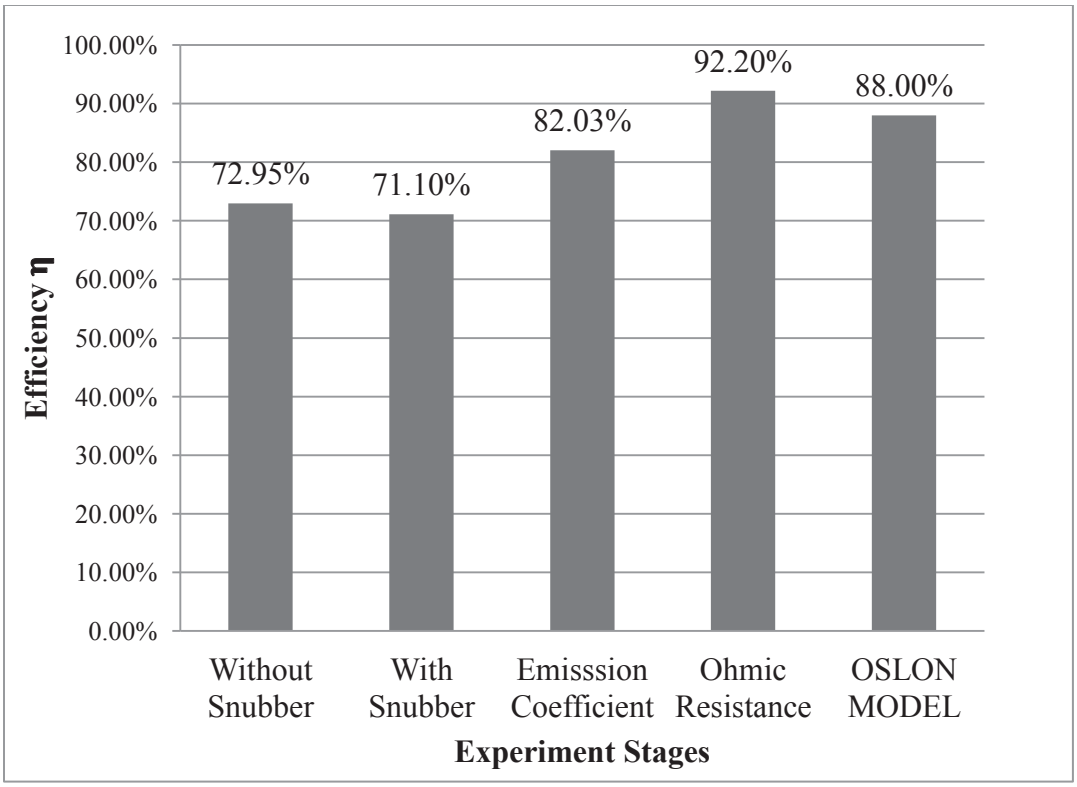

Figure 433: Efficiency graph at different experiment stages

Using the commercial LED model with Driver circuit 2 resulted in an efficiency value very close to the one that is obtained by modeling the LED Ohmic resistance. The above model has an optical efficiency of 89 Lm/W.

Chapter 5

Conclusion and Future Work

5.1 Conclusion

In this thesis the design of an efficient LED dimming driver is presented. This work features the three separate driver designs and their advantages using PWM as the means to control the brightness of LEDs. The SPICE model parameters of LEDs and MOSFET are used in modeling the LEDs for increasing the efficiency of operation.

After designing the basic driver for LEDs, snubber circuit is designed to eliminate the spikes caused by the parasitic elements across the terminals of the power MOSFET. Separate Snubber circuits are designed for these driver circuits and their functionality is discussed in detail. Trapezoidal rule is used in calculating the efficiency at which these driver circuits are operating. The individual circuit efficiencies obtained after inserting the Snubber circuits are compared to choose the optimum driver. Modeling LED parameters such as emission coefficient and ohmic resistance improve the efficiency to 92%. In order to determine the feasibility of the designed driver with the real-world commercial LEDs, the PSpice models of the proposed LEDs are replaced with an OSLON LED model. The efficiency of operation was close to 88% which is quite close to the one obtained earlier.

5.2 Future Work

A prototype of a dimming driver with RGB LEDs can be constructed and analyzed based on this SPICE model. The rise time of the waveform obtained after plugging in the Snubber circuit can be reduced to increase the reaction time. A control algorithm can be designed to control the switching cycles of the MOSFET. The higher level MOSFET can be utilized to increase the accuracy of the simulation and decrease the infrequent convergence problems. The frequency domain of these designed drivers can be expanded further.

Bibliography

[1] Y. T. Huang, Y. T. Chen, Y. H. Liu, H. C. Hsiao and W. T. Tsai, "Compact-Size and High-Conversion-Efficiency Regulator for Alternating-Current-Operated Light-Emitting Diodes," *IEEE Trans. Ind. Electron,* vol. 58, no. 9, pp. 4130-4135, Sep.2011.

[2] C. Y. Wu, T. F. Wu, J. R. Tsai, Y. M. Chen and C. C. Chen, "Multistring LED backlight driving system for LCD panels with color sequential display and area control," *IEEE Trans. Ind. Electron,* vol. 55, no. 10, pp. 3791-3800, Oct. 2008.

[3] S. C. Tan, "General n-level driving approach for improving electrical-tooptical energy-conversion efficiency of fast response saturable lighting devices," *IEEE Trans. Ind. Electron,* vol. 57, no. 4, pp. 1342-1353, Apr. 2010.

[4] H. J. Chiu, Y. K. Lo, T. P. Lee, S. C. Mou and H. M. Huang, "Design of an RGB LED backlight circuit for liquid crystal display panels," *IEEE Trans. Ind. Electron,* vol. 56, no. 7, pp. 2793-2795, Jul. 2009.

[5] Y. K. Lo, K. H. Wu, K. J. Pai and H. J. Chiu, "Design and implementatiom of RGB LED drivers for LCD backlight modules," *IEEE Trans. Ind. Electron,* vol. 56, no. 12, pp. 4862-4871, Dec. 2009.

[6] J. Y. Tsao, "Solid-state lighting: Lamps, chips and materials for tomorrow," *IEEE Circuits Devices Mag,* vol. 20, no. 3, pp. 28-37, May 2004.

[7] H. J. Chiu, Y. K. Lo, J. T. Chen, S. J. Cheng and S. C. Mou, "A high efficiency dimmable LED driver for low-power lighting applications," *IEEE Trans. Ind. Electron,* vol. 57, no. 2, pp. 735-743, Feb. 2010.

[8] D. Cooper, "Dimming LED lighting," AEG Power Solutions, Plano, Nov 2011.

[9] C. Glaser, "Analog technique simplifies LED dimming in portable applications," *LEDs Magazine,* 1 Nov 2011.

[10] DALI - a working party of ZVEI, "DALI," ZVEI-Division Luminaires, Sept 2001. [Online]. Available: http://www.dali-ag.org/. [Accessed 13 Mar 2013].

[11] PLASA, "PLASA," ESTA-PLASA, Jan 1998. [Online]. Available: https://www.plasa.org/. [Accessed 16 Mar 2013].

[12] ZigBee Alliance, "ZigBee," May 2003. [Online]. Available: https://www.zigbee.org/.

[Accessed 25 Jan 2013].

[13] L. W. Nagel, "The Life of SPICE," 30 Sep 1996. [Online]. Available: http://www.designers-guide.org/Perspective/life-of-spice.pdf. [Accessed 21 Jan 2013].

[14] Cadence, "Cadence OrCAD Solutions," 1988. [Online]. Available: http://www.cadence.com/products/orcad/orcad_capture/pages/default.aspx. [Accessed 23 Apr 2013].

[15] H. T. Russell Jr, "The SPICE Diode Model," San Jose, Aug 1991, pp. 1-39.

[16] P. D. Mitcheson, "SPICE Diode and BJT models - Semiconductor Modelling in SPICE," Department of Electrical and Electronic Engineering Imperial College London, London, 2011.

[17] C. R. Wie, "Semiconductors and Microelectronic Devices Educational Applets," University of Buffalo, NY, July 1996. [Online]. Available: http://www.acsu.buffalo.edu/~wie/applet/spice_pndiode/spice_diode_table.html. [Accessed 25 Apr 2013].

[18] SYNOPSYS, HSPICE MOSFET Models Manual, Mountain View, CA: Synopsys, Inc., Sept 2005.

[19] J. V. d. Spiegel, "SPICE model parameters of MOSFETS," 4 Sept 1997. [Online]. Available: http://www.seas.upenn.edu/~jan/spice/spice.MOSparamlist.html. [Accessed 4 Mar 2013].

[20] L. R. Tuladhar, "Resonant power MOSFET drivers for LED lighting," M.S. thesis, Youngstown State University, Youngstown, OH, 2009.

[21] Electrical and Computer Engineering Dept - CMU, "Analysis and Design of Digital Integrated Circuits (18-322) - Lecture 4," Carnegie Mellon University, Pittsburgh, PA, 2003.

[22] R. W. Erickson and D. Maksimovic, Fundamentals of Power Electronics, New York: Kluwer Academic Publishers, 2001.

[23] A. Sattar, "Power MOSFET Basics," IXYS Corporation, Milpitas, CA, 2012.

[24] J. Dodge, "Power MOSFET Tutorial," Advanced Power Technology, Bend, OR, Mar 2006.

[25] C. Spielman and M. M. Budnik, "MOSFETs, High Side Drivers, and Low Side Drivers,," BTIP - Valparaiso's University, Valparaiso, IN, July 2008.

[26] A. A. Boora, F. Zare and A. Ghosh, "Efficient voltage/current spike reduction by active gate signaling," *in Electromagnetic Compatibility Symposium,* pp. 59-64, Sept. 2009.

[27] Q. I. Rahman and G. Schmeisser, "Characterization of the speed of convergence of the trapezoidal rule," *Numerische Mathematik,* vol. 57, no. 1, pp. 123-138, 1990.

[28] J. A. C. Weideman, "Numerical Integration of Periodic Functions: A Few Examples," *The American Mathematical Monthly,* vol. 109, no. 1, pp. 21-36, Jan. 2002.

[29] P. Dawkins, "Paul's Online Math Notes," 21 Feb 2012. [Online]. Available: http://tutorial.math.lamar.edu/Classes/CalcII/ApproximatingDefIntegrals.aspx. [Accessed 23 Dec 2013].

[30] R. Severns, "Design of Snubbers for power circuits," 10 Mar 2010. [Online]. Available: http://www.cde.com/tech/design.pdf. [Accessed 05 Feb 2013].

[31] N. Chowdhury, "Notes on Snubber Circuits - EE 443 Power Electronics," College of Engineering, University of Saskatchewan, Saskatoon, Canada, Jan 2013.

[32] R. Schmitt, "ELECTRODYNAMICS," in *Electromagnetics Explained*, Burlington, MA, Elsevier Science, 2002, p. 75.

[33] OSRAM Opto Semiconductors, "Reliability of the OSLON product Family," OSRAM OS, Regensburg, Germany, Mar 2012.

[34] G. B. Stringfellow and M. G. Craford, "High Brightness Light Emitting Diodes" Semiconductors and Semimetals, San Diego: Academic Press, 1997.

[35] J. Hagerman, "Calculating Optimum Snubbers," Hagerman Technology, Honolulu, HI, July 1995.

[36] K. Ackerson, "Analog Electronics Tutorial Series - Diodes," Virginia Tech EE, Blacksburg, VA, Spring 2002.

[37] SYNOPSYS, "SYNOPSYS - HSPICE," 1986. [Online]. Available: http://www.synopsys.com/tools/Verification/AMSVerification/CircuitSimulation/HSPICE/Pages/default.aspx. [Accessed Apr 2013].